Algal lipid distributions and hydrogen isotope ratios reflect phytoplankton community dynamics

Antonia Klatt[1], Cindy De Jonge[2], Daniel B. Nelson[3], Marta Reyes[4], Carsten J. Schubert[5,6], Nathalie Dubois[2,7] & S. Nemiah Ladd[1]*

[1]University of Basel, Department of Environmental Sciences, Organic Geochemistry, Basel, Switzerland (antonia.klatt@unibas.ch)

[2]ETH Zurich, Department of Earth Sciences, Zurich, Switzerland

[3]University of Basel, Department of Environmental Sciences, Botany, Basel, Switzerland

[4]Swiss Federal Institute of Aquatic Science and Technology (Eawag), Department Aquatic Ecology, Dübendorf, Switzerland

[5]Swiss Federal Institute of Aquatic Science and Technology (Eawag), Department Surface Waters – Research and Management, Kastanienbaum, Switzerland

[6]ETH Zurich, Department of Environmental System Science, Zurich, Switzerland

[7]Swiss Federal Institute of Aquatic Science and Technology (Eawag), Department Surface Waters – Research and Management, Dübendorf, Switzerland

*corresponding author n.ladd@unibas.ch, +41 61 207 36 36

This is a non-peer-reviewed preprint submitted to EarthArXiv. This manuscript has been submitted for peer review at *Geochimica et Cosmochimica Acta*.

Abstract

Reconstructions of past changes in algal community composition provide important context for future alterations in biogeochemical cycling. However, many existing phytoplankton proxies are indicative of individual algal groups and are not fully representative of the whole community. Here, we evaluated hydrogen isotope ratios of algal lipids (δ^2H_{lipid}) as a potential proxy for phytoplankton community composition. We sampled the water column of Rotsee, a small eutrophic lake in Switzerland, every second week from January 2019 to February 2020 and analyzed distributions and the relative offsets between δ^2H_{lipid} values ($\varepsilon^2_{Lipid1/Lipid2}$) from short-chain fatty acids, phytosterols and phytol. Comparing these data with phytoplankton cell counts, we found $\varepsilon^2_{C16:0/sterol}$ and $\varepsilon^2_{sterol/phytol}$ values reflect shifts in the eukaryotic algal community. To assess whether the selected phytoplankton groups were the main sources of the selected lipids, we further modeled algal $\varepsilon^2_{Lipid1/Lipid2}$ values based on $\delta^2H_{C16:0}$, δ^2H_{sterol} and δ^2H_{phytol} values from batch cultures of individual algal groups and their biovolume in Rotsee and evaluated the role of heterotrophy on $\varepsilon^2_{Lipid1/Lipid2}$ values using a model incorporating $\delta^2H_{C16:0}$ and δ^2H_{sterol} values from microzooplankton. Annually-integrated and amount-weighted $\varepsilon^2_{Lipid1/Lipid2}$ values measured in Rotsee were within 6 to 17 ‰ of the mean of modeled algal $\varepsilon^2_{Lipid1/Lipid2}$ values, demonstrating a strong link with the phytoplankton community composition, while $\varepsilon^2_{Lipid1/Lipid2}$ values including microzooplankton lipids had a larger offset. Additionally, cyanobacterial biovolume was positively correlated with the ratio of phytol and phytosterols (phytol:sterol ratio) as well as the ratio of unsaturated C18 and C16:0 fatty acids (C18:C16 ratio). Our results support the application of sedimentary $\varepsilon^2_{Lipid1/Lipid2}$ values in eutrophic lakes as a proxy for past phytoplankton community assemblages. Moreover, the calculation of sedimentary phytol:sterol and C18:C16 ratios provides an additional proxy for reconstructing cyanobacterial blooms.

Key words: Algae, lipid biomarkers, hydrogen isotopes, eutrophic lakes

1. Introduction

In recent decades, temperate lakes have been increasingly impacted by anthropogenic eutrophication and climate change, leading to changes in phytoplankton communities (e.g., Shimoda *et al.*, 2011; McGowan *et al.*, 2012; Callisto *et al.*, 2014; Huisman *et al.*, 2018; Lin *et al.,* 2021). The composition of lacustrine phytoplankton communities greatly impacts biogeochemical cycling of carbon, nitrogen, and phosphorus (Ptacnik *et al.,* 2008; Litchman *et al.*, 2015; Naselli-Flores & Padisák, 2023), as well as higher trophic levels in aquatic food webs (e.g., Wacker & Martin-Creuzberg 2012). To predict future changes in phytoplankton community composition, modeling approaches incorporate results from culturing studies and observations of algal responses to biotic and abiotic factors (e.g., Arhonditsis *et al.,* 2006, Acevedo-Trejos *et al.,* 2015; Henson *et al.,* 2021; Mattern *et al.*, 2022; Liu *et al.,* 2023). However, long-term impacts of climate and environmental changes are difficult to replicate in algal cultures and short-term community feedbacks. Therefore, reconstructions of past phytoplankton community changes over longer timescales (decades, centuries, millennia) offer important insights for modeling future dynamics (e.g., Cvetkoska *et al.,* 2021).

Diverse proxies for estimating past phytoplankton community compositions exist, each associated with its own limitation and biases. For instance, paleolimnologists often quantify the abundance of dinoflagellate cysts or diatom silicate frustules (e.g., Dale & Fjellså 1994; Lotter 1998; Hinder *et al.,* 2021; Cvetkoska *et al.,* 2021), but only limited taxa produce fossil remains, so these are not representative of the whole community. Other reconstructions are based on pigments (e.g., Leavitt 1993; Reuss *et al.*, 2005), or sedimentary ancient DNA (*sed*aDNA) (Capo *et al.,* 2022), two compound classes that can be impacted by degradation and associated preferential diagenesis (Reuss *et al.,* 2005; Capo *et al.,* 2015; Nwosu *et al.,* 2023; Thorpe *et al.,* 2024)

Due to their good preservation over geological times, algal membrane lipids in sediments and rocks have been used to trace past phytoplankton abundance (e.g., Schubert *et al.,*

1998; Naeher *et al.,* 2012; Brocks *et al.,* 2017; Summons *et al.,* 2022; Zeman-Kuhnert *et al.,*2023). For example, eukaryotic and bacterial membranes contain saturated and unsaturated short-chain fatty acids, such as C16:0, C16:1, C18:0, C18:1 or C18:3 (Killops & Killops 2004; Rustan & Drevon 2005; Li *et al*., 2010; Taipale *et al*., 2013). Additionally, eukaryotes modify membrane fluidity and permeability by the incorporation of sterols (Volkman 2003; Dufourc 2008; Desmond & Gribaldo 2009). Typical sterols of photoautotrophic eukaryotes, i.e., plants and microalgae, are brassicasterol (24-methylcholesta-5,22-dien-3β-ol), stigmasterol (24-ethylcholesta-5,22-dien-3β-ol) and sitosterol (24-ethylcholest-5-en-3β-ol) (Killops & Killops 2004; Piironen *et al.,* 2000; Taipale *et al.,* 2016; Peltomaa *et al.,* 2023). Despite bacterial gene homologues potentially encoding enzymes involved in sterol synthesis (Wei *et al.,* 2016), cyanobacteria have been found to generally lack any sterols (e.g., Volkman 2003; Martin-Creuzburg *et al.,* 2008; Taipale *et al.,* 2016; Peltomaa *et al.,* 2023). In addition to membrane lipids, phytol ((2E,7R,11R)-3,7,11,15-Tetramethyl-2-hexadecen-1-ol), the ester-linked side-chain of chlorophyll, is preserved in sediment and interpreted as lipid biomarker for all phototrophs (e.g., Rontani & Volkman 2003; Killops & Killops 2004; Witkowski *et al.,* 2020). Some compounds have been used as proxies for specific phytoplankton groups (e.g., Mouradian *et al.,* 2007; Yuan *et al.,* 2020), but many lipids are not as source-specific as initially thought (e.g., Rampen *et al.,* 2010). Rather than focusing on source-specific biomarkers, a more holistic analysis of lipid distributions might highlight shifts in the phytoplankton community with a greater robustness.

In addition to the variability in lipid biomarkers, phytoplankton community composition might be reflected in the hydrogen isotope ratios of algal lipids, i.e., δ^2H_{lipid} values ($\delta^2H = ({}^2H/{}^1H)_{sample}/({}^2H/{}^1H)_{VSMOW} - 1$). Initially considered as a proxy for δ^2H values of past lake water (e.g., Sauer *et al.,* 2001; Huang *et al.,* 2004), algal δ^2H_{lipid} values have been found to be impacted by algal growth rate, salinity, temperature and CO_2 limitation (e.g., Z. Zhang *et al.,* 2009; Sachs & Schwab 2011; Nelson & Sachs 2014; Sachs & Kawka 2015; Torres-Romero *et al.,* 2024) and there is increasing evidence of a strong ecological signal recorded in algal δ^2H_{lipid} values. For instance, δ^2H_{lipid} values vary significantly among different algal

groups grown under identical conditions in laboratory cultures (Schouten *et al.,* 2006, Zhang & Sachs 2007; M'Boule *et al.,* 2014; Heinzelmann *et al.,* 2015; Ladd *et al.,* 2024).

Yet, changes in δ^2H values of lake water might still be recorded in algal lipids as the hydrogen for lipid synthesis originates from source water (e.g., Sachse *et al.*, 2012). By using relative offsets between δ^2H_{lipid} values (i.e., $\varepsilon^2_{Lipid1/Lipid2} = (\delta^2H_{Lipid1}+1)/(\delta^2H_{Lipid2}+1) - 1$), the potential isotopic signal from lake water is excluded. Culturing and mesocosm experiments have shown that $\varepsilon^2_{Lipid1/Lipid2}$ values strongly differ among different phytoplankton groups (Ladd *et al.,* 2024). For example, $\varepsilon^2_{C16:0/phytol}$ values for green algae and cyanobacteria were up to 150 ‰ higher than for diatoms, cryptomonads and dinoflagellates, while $\varepsilon^2_{C16:0/sterol}$ values for diatoms were > 250 ‰ lower than for green algae. This ecological range in algal δ^2H_{lipid} values exceeds the difference between δ^2H values of precipitation in the subtropics and boreal zones (e.g., Darling *et al*., 2006), as well as changes in isotopic precipitation signatures during glacial/interglacial cycles (e.g., Vimeux *et al*., 1999; Osman *et al.,* 2021).

In this study, we evaluated $\varepsilon^2_{Lipid1/Lipid2}$ values as a proxy for phytoplankton community composition in a natural lacustrine system and sought to improve the reconstruction of algal communities based on holistic analyses of lipid biomarker distributions. For this aim, samples were taken from the water column of Rotsee, a small eutrophic lake in central Switzerland, every second week from January 2019 to February 2020. Cell counts of phytoplankton and microzooplankton were conducted and lipid abundances as well as compound-specific δ^2H_{lipid} values of short-chain fatty acids, sterols and phytol were measured. We compared $\varepsilon^2_{Lipid1/Lipid2}$ values and lipid distributions to phytoplankton biovolume to assess how lipid-based indicators captured algal community shifts throughout the year. Specifically, we analyzed whether cyanobacterial and green algal blooms are reflected by $\varepsilon^2_{C16:0/phytol}$ values and if changes in the eukaryotic algal community composition can be inferred from $\varepsilon^2_{C16:0/sterol}$ and $\varepsilon^2_{sterol/phytol}$ values. Furthermore, $\varepsilon^2_{Lipid1/Lipid2}$ values incorporating biovolume-weighted δ^2H_{lipid} values from microzooplankton were modeled to investigate potential heterotrophic signatures in $\varepsilon^2_{Lipid1/Lipid2}$ values.

2. Methods

2.1 Study site and sample collection

Rotsee is a small (0.47 km^2 surface area), monomictic and eutrophic lake in central Switzerland (47°04′11″N 8°18′51″E) (Fig. 1) at 419 m asl (Bloesch 1974; Lotter 1989). The maximal depth is 16 m with a total volume of $4.3x10^6$ m^3 (Bloesch 1974). During the one-year sampling period, depth profiles of turbidity, conductivity, temperature, pH and dissolved oxygen were measured by different multi-parameter CTD probes (75M, Sea and Sun Marine Tech, Trappenkamp, Germany; WTW, Weilheim, Germany). Temperatures at specific sampling depths were estimated by the mean of temperatures from 0.5 m above to 0.5 m below the respective depth.

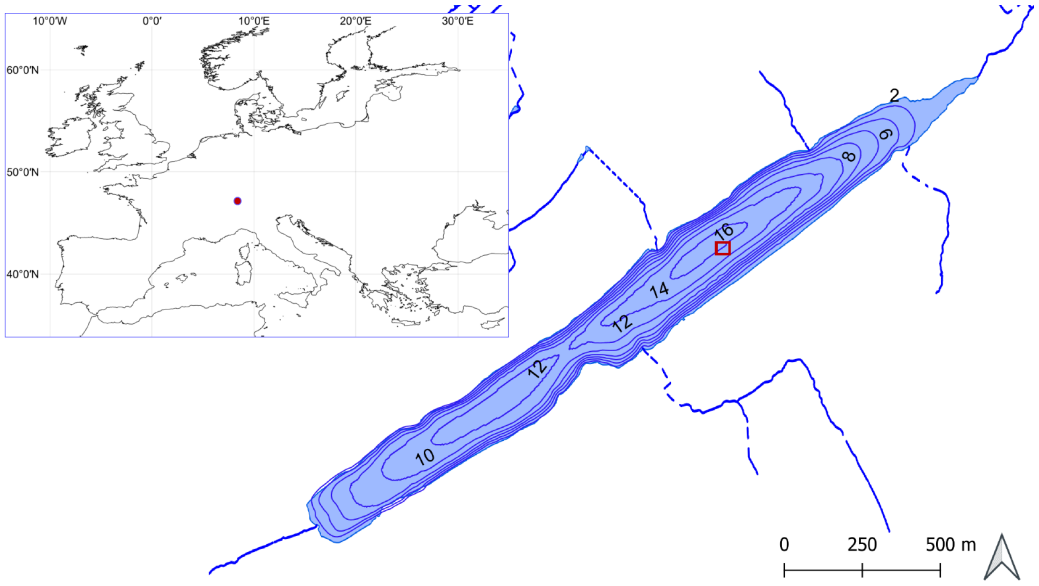

Figure 1: Location of Rotsee (red point) and schematic image indicating the sampling area (red box) near the center of the lake. European coastlines were accessed from Natural Earth (https://www.naturalearthdata.com). River connections and bathymetric map of Rotsee were accessed from swissTLM3D and DHM25 (swisstopo.admin.ch) (DHM25 data modified from T. Doda). All maps were produced with QGIS Geographic Information System.

Sampling occurred every second week near the lake's center (Fig. 1) from January 2019 to February 2020 on mostly sunny mornings. Samples were taken at 1 m depth and at the depth of chlorophyll maximum, as determined based on the turbidity maximum on the respective sampling date measured by the multi-parameter CTD probe. Chlorophyll maximum depths ranged from 5 m to 14 m. If no turbidity maximum was present, samples were collected at 4 m depth. Lake water was filtered through a pre-combusted (6 hours at 450 °C) 142 mm Whatman® GF/F filter (pore size 0.7 µm) with a WTS-LV Large Volume Pump (12-40 l; McLane, MA, USA). Filters were wrapped in pre-combusted aluminum foil, kept on ice during transport, and stored at -20 °C until further analysis. Water samples for phytoplankton, water isotope measurements and nutrient analyses were collected with a Niskin Water Sampler at the same depths (5 l; Hydro-Bios, Altenholz, Germany). For phytoplankton samples, 40 ml water were directly fixed with 5 ml lugol solution (5% iodide, 10% potassium iodide) and stored in the dark at 4°C until identification, which occurred within a few weeks. For water isotope samples, 2 ml water were filtered through a 25 mm syringe filter with a 0.45 µm polyethersulfone membrane into 2 ml vials and stored at 4 °C prior to analysis. Samples for nutrient analysis were filtered through cellulose acetate (pore size 0.45 µm) and stored in opaque bottles at 4 °C prior to analysis.

2.2 Nutrient concentrations

Total phosphorous concentrations were measured according to Vogler (1965) with modifications. Following chemical digestion with potassium peroxodisulfate at 121 °C, ortho-phosphate concentrations were determined after the reaction to a phosphorus-molybdenum-blue-complex with a spectrophotometer (Cary 60, Agilent, Santa Clara, CA, USA). Total nitrogen concentrations were measured by chemiluminescence with a Total Organic Carbon Analyzer with Total Nitrogen Unit (TOC-L CSH, Shimadzu, Nakagyo-ku, Kyōto, Japan).

2.3 Microscopy and biovolume calculation

A sub-sample (3 ml or 10 ml depending on density) was sedimented and counted in an Utermöhl-chamber (Hydro-Bios) (von Utermöhl, 1931). Phytoplankton were identified and counted using an inverted microscope (Zeiss Axiovert 135, Carl Zeiss, Oberkochen, Germany) at 320x and 640x. Identifications were performed to the greatest possible taxonomic level (generally genus or species). The abundance of rare species which did not appear in the counted fields (40 in each magnification), was estimated in a transect at a magnification of 320x. Cell densities were normalized to an appropriate volume (cells/l) and the biovolume of different phytoplankton groups was calculated by multiplying the cell densities of the corresponding species by their mean per-cell biovolume. Biovolume values were based on biovolume measurements from individual phytoplankton cells from Greifensee according to standard protocols (Narwani *et al.,* 2019).

2.4 Lipid extraction and quantification

All glassware and utensils used for lipid extraction and purification were pre-combusted or solvent-cleaned with dichlormethane (DCM):methanol (MeOH) (9:1 (v/v)).

Total lipid extracts (TLEs) for fatty acid and phytol analyses were extracted from half of a freeze-dried filter sample in a SOLVpro microwave reaction system (Anton Paar, Graz, Austria) according to Ladd *et al.* (2017) with the same internal standard. TLEs for sterol analyses were extracted from the other half of the dry filter sample with an accelerated solvent extraction system (ASE) (Dionex™ ASE™ 350, Thermo Fisher Scientific, Waltham, MA, USA) according to Hirave *et al.* (2021). Prior to ASE extractions, an internal standard containing heneicosanol (*n*-C_{21}-alkanol), hexatriacontane (*n*-C_{36}-alkane), nonadecanoic acid (*n*-C_{19}-acid) and 2-octadecanone was quantitatively added to each sample.

TLEs were saponified with ~ 3 ml 1 N potassium hydroxide (KOH) in MeOH for 3-16 hours at 70 °C. After saponification, 2 ml of MilliQ water was added to each sample and the

neutral fraction was extracted using multiple heptane rinses. The aqueous phase containing the acid fraction was acidified to pH < 2 and the protonated acid fraction was extracted using multiple heptane rinses.

A subset of neutral fractions was further purified by silica gel column chromatography according to Ladd *et al*. (2017) to obtain the alcohol fraction, but as no compounds were present in the other fractions, alcohols were subsequently analyzed in unpurified neutral fractions. The neutral or alcohol fraction was acetylated with 200 µl pyridine and 25 µl acetic anhydride for 30 min at 70 °C. The δ^2H values of the added acetyl group were determined by mass balance calculation after the acetylation of *n*-C_{21}-alkanol or sucrose with a known δ^2H value. Additionally, δ^2H values of acetic anhydride were further measured on a high-temperature conversion/elemental analyzer (TC/EA) (Thermo Fisher Scientific) coupled to a Delta V plus isotope ratio mass spectrometer (IRMS) (Thermo Fisher Scientific) *via* a ConFlo IV interface (Thermo Fisher Scientific) following Newberry *et al.* (2017).

Acid fractions were methylated with 4 ml 95:5 MeOH:hydrochloric acid (HCl) at 70 °C for ~ 16 hours. Methylated samples were mixed with 4 ml of 0.1 M potassium chloride (KCl) in MilliQ water and fatty acid methyl-esters (FAMEs) were extracted by serial heptane rinses. The δ^2H value of the added methyl group was determined by mass balance calculation after the methylation of phthalic acid of a known δ^2H value (Arndt Schimmelmann, Indiana University).

Acetylated alcohols (phytol and sterols) and FAMEs were quantified by gas chromatography–flame ionization detection (GC-FID) on a Trace™ 1310 gas chromatograph (Thermo Fisher Scientific) with a Rtx-5MS Column (30 m x 0.25 mm x 0.25 µm) (Restek, Bad Homburg vor der Höhe, Germany) according to Baan *et al.* (2023). Sterols and phytol were initially identified by analyzing the mass spectra of a subset of samples by gas chromatography-mass spectrometry (GC-MS) according to Ladd *et al.* (2017). An equivalent column was used for GC-FID analyses, and sterols and phytol were identified based on their elution order and relative peak areas. FAMEs were identified by comparing retention times to

239 an external standard (Sulpelco® 37-component FAME Mix, reference no. 47885U) (Merck
240 KGaA, Darmstadt, Germany).
241

242 ## 2.5 Lipid δ^2H measurements

243 Lipid δ^2H values were measured by gas chromatography-isotope ratio mass spectrometry
244 (GC-IRMS) on a Trace GC Ultra (Thermo Fisher Scientific) coupled to a Delta V plus IRMS
245 (Thermo Fisher Scientific) with a ConFlo IV interface (Thermo Fisher Scientific). Samples
246 were injected with an AS TriPlus autosampler (Thermo Fisher Scientific) to a split/splitless
247 inlet operated in splitless mode at 280 °C. FAMEs were measured on a Rtx-2330 column (30
248 m x 0.25 mm x 0.20 µm) (Restek), which was heated from 60 to 130 °C at 15 °C/min, from
249 130 to 265 °C at 8 °C/min and held at 265 °C for 5 min. Alcohols were measured on a Rtx-
250 5MS column (30m x 0.25mm x 0.25µm) (Restek) which was heated from 60 to 120 °C at 15
251 °C/min, from 120 to 325 °C at 5 °C/min and held at 325 °C for 10 min. Column effluent was
252 pyrolyzed at 1420 °C.

253 Measured hydrogen isotope values from the Thermo Isodat 3.0 software were converted
254 to the Vienna Standard Mean Ocean Water (VSMOW) scale with regression models between
255 measured and externally provided δ^2H values for reference standard compounds, which
256 were analyzed at the beginning and the end of each sequence and between at most ten
257 sample injections. Normalization included an initial linear regression between measured and
258 known δ^2H values and a second multiple linear regression to correct for drift and isotopic
259 effects related to peak size and retention time. Reference standards included *n*-alkane Mix
260 A7 and FAME Mix F8-3 (Arndt Schimmelmann, Indiana University), and C20:0 FAME
261 USGS71 (United States Geological Survey).

262 δ^2H_{sterol} values were further corrected for biases related to peak dimensions due to
263 variable size effects between sterols and the aliphatic standards. Cholesterol acetate and
264 stigmasterol acetate stock compounds (Merck) were measured at different concentrations
265 ranging from 50 ng to 2 µg to determine the threshold peak area for stable δ^2H values, which

was ~ 40 Vs (Fig. S1A). δ^2H values of the same stock compounds were separately calibrated on a TC/EA IRMS (Thermo Fisher Scientific) according to Newberry *et al.* (2017) (cholesterol acetate) or as the average of δ^2H values at appropriate peak areas (stigmasterol acetate). The resulting relationship between peak area and the relative isotopic offset between measured and calibrated δ^2H values ($\varepsilon^2_{measured/calibrated}$) (Fig. S1B) was used to correct δ^2H_{sterol} values based on their individual peak areas.

Quality control standards (*n*-$C_{29,32}$ alkanes (Stable Isotope Ecology Laboratory, University of Basel); C20:0 FAME (USGS70, United States Geological Survey); Supelco® C8-C24 FAME Mix (reference no CRM18918, Merck)) were measured throughout each sequence and scale normalized to VSMOW in the same way as the samples. Of these, the *n*-C_{32} alkane and the C20:0 FAME were purchased isotope reference materials with known δ^2H values, while δ^2H values of the remaining compounds have been routinely measured to track long term measurement precision. The average standard deviation (SD) for all quality control compounds together was 2 ‰, with an average offset of 0.4 ‰ from their known value (n = 467). The H_3^+ factor was determined in the beginning of each sequence and averaged 2.8 +/- 0.2 ppm nA^{-1}. Sample δ^2H values were further corrected for hydrogen added during derivatization based on isotopic mass balance. Errors were estimated from replicate measurements and the uncertainties associated with the added hydrogen.

2.6 Water δ^2H measurements

Water δ^2H values were measured on a TC/EA IRMS (Thermo Fisher Scientific) according to Newberry *et al.* (2017). Two water standards with known δ^2H values were injected at the beginning and the end of each sequence and after every 14 sample injections. Values were normalized to the VSMOW scale using measured and known δ^2H values of laboratory working standards and included corrections for time-based drift and memory effects. As a quality control, another water standard was injected at the beginning and the end of each

sequence and after every 14 sample injections and corrected in the same way as the samples. The SD of the standard averaged 0.26 ‰ and the average offset from the known value was 0.05 ‰.

2.7 Calculations & statistics

Statistical analyses and modeling of $\varepsilon^2_{Lipid1/Lipid2}$ values were carried out in R (R version 4.3.1, R Core Team 2023, Vienna, AT) and RStudio (2023.06.1+524). If not stated otherwise, the 'ggplot2' (Wickham 2009) and the 'cowplot' package (Wilke 2020) were used for visualizations.

2.7.1 Modeling of $\varepsilon^2_{Lipid1/Lipid2}$ values

We simulated algal $\varepsilon^2_{Lipid1/Lipid2}$ values with a 50,000 iteration Monte Carlo model based on the hydrogen isotope fractionation between different algal lipids and source water ($\alpha^2_{lipid/water}$ = ($^2H/^1H_{lipid}$)/($^2H/^1H_{water}$)) calculated from previously published culture experiments as well as the relative contribution of each algal group to the lipid pool. Detailed model specifications for the modeling of biweekly $\varepsilon^2_{Lipid1/Lipid2}$ values can be found in the R code available in GitHub (https://github.com/antoniaKlatt/Klatt_etal_2024_phytoplankton_Rotsee).

Specifically, theoretical normal distributions of $\alpha^2_{lipid/water}$ values were estimated for each algal group and lipid based on mean $\alpha^2_{C16:0/water}$, $\alpha^2_{sterol/water}$ and $\alpha^2_{phytol/water}$ values with corresponding standard deviations (SD) derived from batch cultures of *Cyanophyceae*, green algae, *Bacillario-, Dino-, and Cryptophyceae* (Ladd *et al.,* 2024) (Fig. S2). No $\alpha^2_{sterol/water}$ values were defined for *Cyanophyceae* as cyanobacteria do not produce any sterols (e.g., Volkman 2003; Martin-Creuzburg *et al.,* 2008; Taipale *et al.,* 2016; Peltomaa *et al.,* 2023). Due to missing culturing data, $\alpha^2_{lipid/water}$ distributions of *Chrysophyceae* were simulated based on $\alpha^2_{lipid/water}$ values from *Bacillario-* and *Dinophyceae* according to their phylogenetic relationship (Not *et al.,* 2021).

318 The three sets of α values predicted from each Monte Carlo simulation were then used to
319 predict sets of $^{2}H/^{1}H_{lipid}$ values for each lipid and algal group based on the $^{2}H/^{1}H_{water}$ value at
320 each sampling date. Then, biovolume-weighted average $^{2}H/^{1}H_{lipid}$ values were calculated for
321 each sampling date by the relative contribution of each algal group to the total phytoplankton
322 biomass for C16:0 and phytol, and the relative contribution of each eukaryotic algal group to
323 total eukaryotic algal biomass for sterols. The three sets of biovolume-weighted average
324 $^{2}H/^{1}H$ values for each lipid were then used to calculate $\varepsilon^{2}_{C16:0/phytol\ phyto}$, $\varepsilon^{2}_{C16:0/sterol\ phyto}$ and
325 $\varepsilon^{2}_{sterolphytol\ phyto}$ values for each sampling date.

326 To model the potential impact of heterotrophic microzooplankton on $\varepsilon^{2}_{Lipid1/Lipid2}$ values, we
327 conducted an additional 50,000 iteration Monte Carlo simulation to estimate theoretical
328 hydrogen isotope fractionation factors between algal and microzooplankton lipids. For this
329 purpose, we used observations of $\delta^{2}H_{C16:0}$ values of seston and zooplankton from Pilecky *et*
330 *al.* (2022) (Fig. S3) and calculated $\alpha^{2}_{seston/zoo}$ values. In this study, seston refers to dietary
331 plankton of < 30 µm from eutrophic ponds (Pilecky *et al.,* 2022) which we used to represent
332 phytoplankton in our calculations. Since empirical $\delta^{2}H_{sterol}$ values from zooplankton were not
333 available, we applied the same set of fractionation factors between seston and zooplankton
334 as that for C16:0 fatty acid.

335 We then simulated $^{2}H/^{1}H_{C16:0}$ and $^{2}H/^{1}H_{sterol}$ values from microzooplankton using
336 biovolume-weighted $^{2}H/^{1}H_{lipid}$ values from phytoplankton and the theoretical $\alpha^{2}_{seston/zoo}$ values.
337 Subsequently, biovolume-weighted $^{2}H/^{1}H_{C16:0}$ and $^{2}H/^{1}H_{sterol}$ values from both phytoplankton
338 and microzooplankton ($^{2}H/^{1}H_{lipid\ phyto\&zoo}$) were calculated by the relative contribution to total
339 biomass or eukaryotic biomass. Then, $\varepsilon^{2}_{Lipid1/Lipid2}$ values representing theoretical contributions
340 from algae and microzooplankton ($\varepsilon^{2}_{Lipid1/Lipid2\ phyto\&zoo}$) were computed using $^{2}H/^{1}H_{lipid\ phyto\&zoo}$
341 values.

342 Seasonal and annual $\varepsilon^{2}_{Lipid1/Lipid2}$ values were calculated with a similar approach to
343 biweekly simulations, but were modified to use seasonal or annual biovolume contributions,
344 and seasonal or annual average water $\delta^{2}H$ values. Detailed model settings for the annual

and seasonal calculations are specified in the R code which is available in GitHub (https://github.com/antoniaKlatt/Klatt_etal_2024_phytoplankton_Rotsee). Average $\varepsilon^2_{Lipid1/Lipid2}$ values from winter 2019 include samples from January and February 2019, while values from winter 2020 include samples from December 2019, January, and February 2020. If no δ^2H_{lipid} value was measurable, the lipid concentration at the specific sampling date was set to zero.

2.7.2 Lipid ratios

Lipid ratios were calculated based on initial lipid concentrations in the water column [µg/L] or based on peak areas in GC-FID measurements [pA*min].

Phytol:sterol ratios were calculated as:

[phytol]/([phytol] +[brassicasterol]+[ergosterol]+[sitosterol]+[stigmasterol]) (1),

and C18:C16 ratios were calculated as:

([C18:1]+[C18:x]+[C18:2]+[C18:3nx])/([C16:0]+[C18:1]+[C18:x]+[C18:2]+[C18:3nx]) (2)

where C18:x represents C18:1n9c co-eluting with C18:2n6t, C18:3nx is C18:3n3 with C18:3n6 and C20:3nx is C20:3n3 with C20:3n6.

2.7.3 Statistical analyses

Spearman's correlation coefficients between $\varepsilon^2_{Lipid1/Lipid2}$ values and the relative biovolume of different phytoplankton groups were calculated using the 'corr.test' function of the 'psych' package (Revelle, 2024) with a Bonferroni adjustment. Correlation matrices were visualized with the 'ggcorrplot' package (Kassambara 2023). Paired two-sided t-tests between modeled $\varepsilon^2_{Lipid1/Lipid2}$ values were performed with the 't.test' function from the 'stats' package (R Core Team 2023, Vienna, AT). Non-metric multidimensional scaling (NMDS) of relative alcohol and fatty acid concentrations was performed with the 'metaMDS' function of the 'vegan'

package (Oksanen *et al.,* 2022) based on Bray-Curtis dissimilarities. Relative concentrations are based on the contribution of individual alcohols to the sum concentrations of all alcohols (excluding cholesterol) on single sampling dates, and the contribution of individual fatty acids to the sum concentrations of all fatty acids (excluding C22:2) on single sampling dates. NMDS of relative alcohol concentrations was performed with untransformed data, while relative fatty acid concentrations were square root transformed. Redundancy Analysis (RDA) between phytoplankton biovolume and environmental variables was performed with the 'rda' function of the 'vegan' package (Oksanen *et al.,* 2022) without scaling of biovolume data. Relative biovolume of phytoplankton groups was square root transformed and total phosphorous concentrations were log transformed prior to RDA. Pearson's correlation between environmental variables were calculated using the 'corr.test' function of the 'psych' package (Revelle 2024). All statistical analyses were performed with complete datasets after removing complete rows containing non-values.

3. Results

3.1 Stratification and vertical mixing in Rotsee

The timing of lake stratification and the onset of autumnal mixing in monomictic Rotsee were assessed by the oxygen and temperature profiles in the water column (Fig. 2). The lake stratification began in spring, and a stable oxycline and thermocline was established between

~ 5 to 10 m depth in summer. Mixing began in October, deepening the thermocline, and no vertical stratification was present by December.

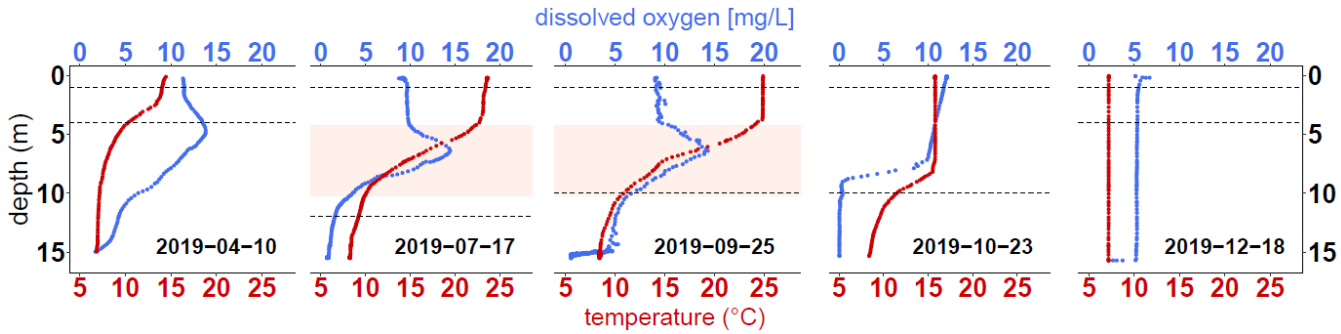

Figure 2: Dissolved oxygen and temperature throughout the water column of Rotsee at different sampling dates representative of different seasons. Only a subset of oxygen and temperature measurements for each date is shown for clarity. The rose-colored areas in summer and early autumn indicate the stable oxycline and thermocline. Dashed lines indicate the respective sampling depths on each sampling date.

3.2 The phytoplankton community is highly dynamic

During the one-year sampling period, diatoms (*Bacillariophyceae*), green algae (*Chloro-* and *Zygnemophyceae*), golden algae (*Chrysophyceae*), cryptomonads (*Cryptopyceae*), cyanobacteria (*Cyanophyceae*), and dinoflagellates (*Dinophyceae*) were identified in varying abundance in Rotsee (Fig. 3). Some phytoplankton blooms were detected concurrently at both sampling depths, for instance, the winter diatom bloom in January 2019, or the major spring bloom of golden algae in April 2019 (Fig. 3A, B). However, some algal blooms were restricted to a certain sampling depth. For example, at 1 m depth, a smaller green algal bloom was detected in February 2019, and a bloom of cryptomonads in late June 2019 (Fig. 3A). At the chlorophyll maximum depth, a first cyanobacterial bloom occurred in late July 2019, followed by a bloom of photosynthetic dinoflagellates in mid-August (Fig. 3B). In October 2019, a massive second cyanobacterial bloom was detected (Fig. 3B), partly overlapping with the lake turnover event (Fig. 2). The cyanobacterial bloom in late October produced the highest absolute algal biovolume during the year.

Besides phytoplankton, various microzooplankton groups were identified, including Ciliata and Rotifera species, as well as the phagocytotic non-photosynthetic dinoflagellate *Gymnodinium helveticum* (Irish 1979; Wille & Hoffmann 1991) (Fig. 3). At 1 m depth, a massive peak of microzooplankton was detected in late July 2019, with Rotifera reaching their maximum biovolume, followed by a Ciliata peak in August (Fig. 3A). The biovolume of Ciliates further increased in late October and mid-December (Fig. 3A). At the chlorophyll maximum depth, a Ciliata peak was detected in February 2019, followed by a massive increase of Ciliates in mid-June (Fig. 3B). The biovolume of *Gymnodinium helveticum* was generally low throughout the year.

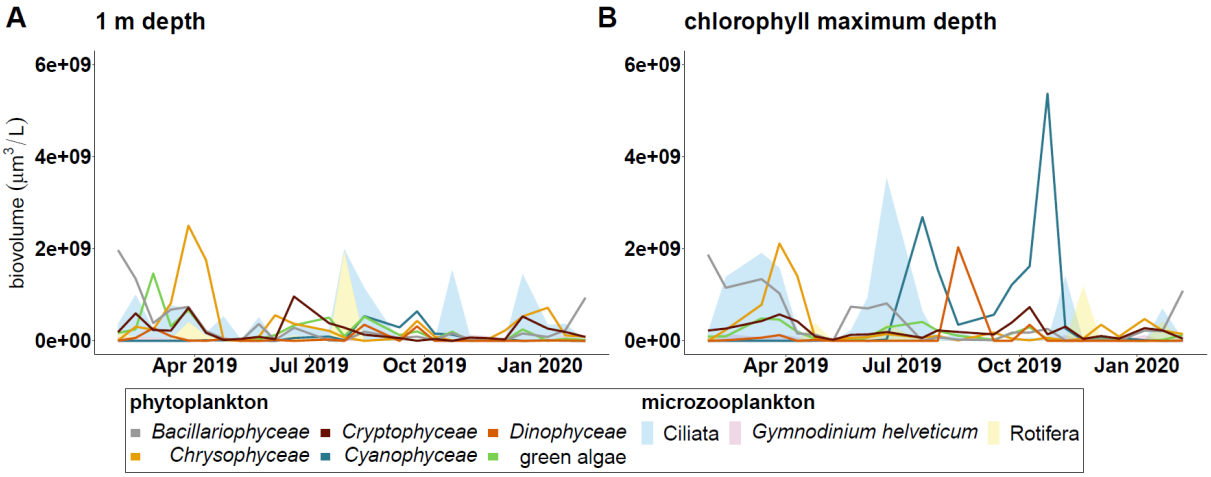

Figure 3: Absolute biovolume of phytoplankton and microzooplankton groups in Rotsee at 1 m depth (A) and chlorophyll maximum depth (B) over time. *Chlorophyceae* and *Zygnemophyceae* were included in the classification 'green algae'.

3.3 δ^2H_{lipid} values generally do not correlate with δ^2H_{water} values

To examine the potential impact of the isotopic signature of lake water on algal δ^2H_{lipid} values in Rotsee, we compared changes of $\delta^2H_{C16:0}$ and δ^2H_{phytol} values with δ^2H_{water} values (Fig. 4). δ^2H_{lipid} values were much more variable than δ^2H_{water} values. Overall, $\delta^2H_{C16:0}$ values spanned a range > 100 ‰ (-304 to -163 ‰) and δ^2H_{phytol} values > 60 ‰ (-434 to -373 ‰), while δ^2H_{water} values only varied between -83 and -76 ‰. At 1 m depth, $\delta^2H_{C16:0}$ values were

significantly positively correlated with δ^2H_{water} values ($R^2 = 0.26$; $p < 0.01$), but not at the chlorophyll maximum depth. δ^2H_{phytol} values were not correlated with δ^2H_{water} values at either depth.

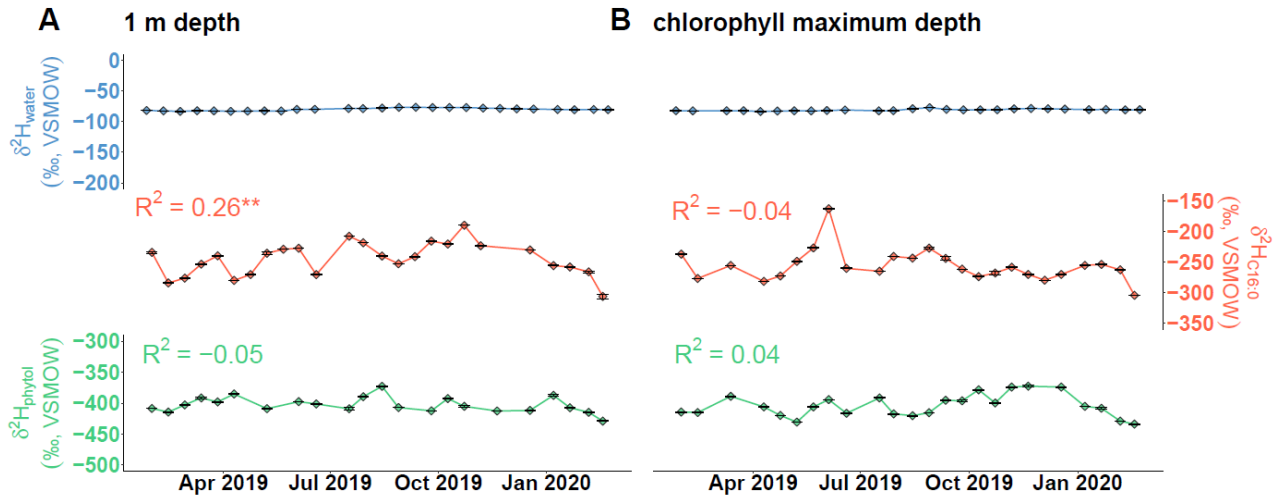

Figure 4: Time series of δ^2H_{water}, $\delta^2H_{C16:0}$ and δ^2H_{phytol} values in Rotsee at 1 m depth (A) and chlorophyll maximum depth (B). R^2 values indicated in each panel refer to linear regressions between δ^2H_{lipid} values and δ^2H_{water} values. **: $P < 0.01$.

Due to low concentrations, δ^2H measurements of sterols were only possible from a subset of sampling dates. The greatest number of measurements were possible from brassicasterol and sitosterol (Fig. S4). Sitosterol was generally the most ^2H-enriched sterol, with δ^2H values ranging from -330 to -216 ‰. The most ^2H-depleted sterol was brassicasterol, which had δ^2H values that ranged from -374 to -286 ‰. δ^2H_{water} values were not correlated with δ^2H_{sterol} values for any sterol at either sampling depth.

3.4 Biweekly relationships between $\varepsilon^2_{Lipid1/Lipid2}$ values and phytoplankton community composition

To assess the fidelity of algal δ^2H_{lipid} values as a proxy for phytoplankton community assemblages, $\varepsilon^2_{Lipid1/Lipid2}$ values were calculated and the relationship between $\varepsilon^2_{Lipid1/Lipid2}$ values and algal community dynamics was analyzed. For late August 2019 and mid-February

2020, no phytoplankton cell counts were available. Due to the small size of our dataset, highly dynamic phytoplankton fluctuations (Fig. 3) and difficulties of extrapolation (Hastie *et al.,* 2009), algal biovolume was not inter-/extrapolated and corresponding lipid samples were excluded from analyses. Moreover, due to missing δ^2H values of different sterols for many sampling dates (Fig. S4), $\varepsilon^2_{C16:0/sterol}$ and $\varepsilon^2_{sterol/phytol}$ values were calculated with weighted average δ^2H_{sterol} values of each sampling date.

There were no significant correlations between $\varepsilon^2_{Lipid1/Lipid2}$ values and the relative biovolume of individual phytoplankton groups, but the direction of some relationships was consistent at both sampling depths (Fig. S5, S6). For instance, green algal biovolume tended to increase with $\varepsilon^2_{C16:0/phytol}$ values (Fig. S5) and diatom biovolume tended to increase with $\varepsilon^2_{sterol/phytol}$ values (Fig. S6).

To assess if phytoplankton community shifts were reflected by $\varepsilon^2_{Lipid1/Lipid2}$ values, the relative biovolume of individual algal groups was combined based on similarities of $\varepsilon^2_{Lipid1/Lipid2}$ values in culturing studies (Ladd *et al.,* 2024) and relationships found in Rotsee (Fig. S5, S6). No relationship between $\varepsilon^2_{C16:0/phytol}$ values and the summed biovolume of cyanobacteria and green algae was found (R^2 = -0.02; $p = 0.6$; Fig. S5). However, the summed biovolume of diatoms and golden algae was negatively correlated with $\varepsilon^2_{C16:0/sterol}$ values ($R^2 = 0.11$; $p < 0.05$) (Fig. 5A) and positively correlated with $\varepsilon^2_{sterol/phytol}$ values ($R^2 = 0.24$; $p < 0.01$) (Fig. 5B). When the linear regressions for these relationships were extrapolated to 100 % diatoms and golden algae, $\varepsilon^2_{sterol/phytol}$ and $\varepsilon^2_{C16:0/sterol}$ values were similar to measurements from diatom cultures (Ladd *et al.*, 2024) (Fig. 5).

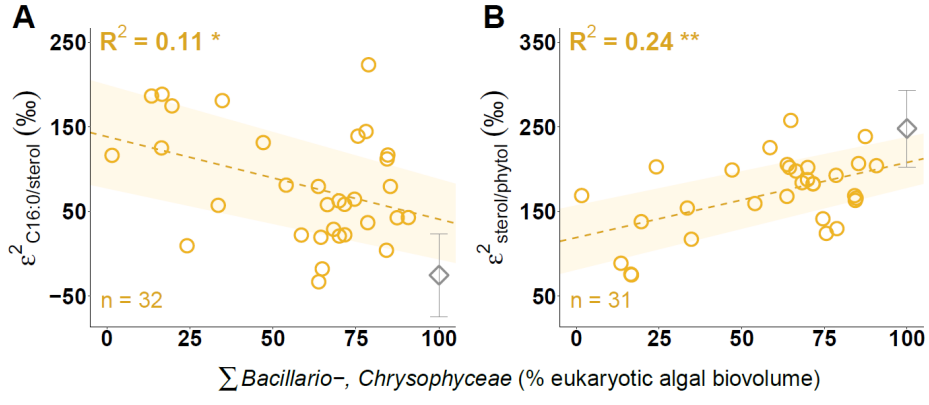

Figure 5: Linear regressions between $\varepsilon^2_{C16:0/sterol}$ (A) and $\varepsilon^2_{sterol/phytol}$ values (B) and the summed relative biovolume of *Bacillario*- and *Chrysophyceae* in Rotsee. Diamond symbols indicate mean $\varepsilon^2_{C16:0/sterol}$ and $\varepsilon^2_{sterol/phytol}$ values from Bacillariophyceae cultures (Ladd *et al.,* 2024), representing theoretical $\varepsilon^2_{Lipid1/Lipid2}$ values at 100% contribution to eukaryotic biovolume. *: $P < 0.05$; **: $P < 0.01$.

To further assess the impact of phytoplankton community composition on $\varepsilon^2_{Lipid1/Lipid2}$ values, measured $\varepsilon^2_{Lipid1/Lipid2}$ values were compared to modeled $\varepsilon^2_{Lipid1/Lipid2}$ values exclusively derived from phytoplankton ($\varepsilon^2_{Lipid1/Lipid2\ phyto}$) (Fig. 6,7), which were simulated based on theoretical δ^2H_{lipid} values of individual algal groups (Ladd *et al.,* 2024) and their biovolume in Rotsee. Moreover, the influence of microzooplankton on the lipid isotopic signal was investigated by simulating $\varepsilon^2_{Lipid1/Lipid2}$ values incorporating biovolume-weighted δ^2H_{lipid} values of phytoplankton and microzooplankton ($\varepsilon^2_{Lipid1/Lipid2\ phyto\&zoo}$). Compared to phytoplankton lipids, lipids of heterotrophs are expected to be more ^{2}H-enriched (e.g., X. Zhang *et al.* 2009; Pilecky *et al.,* 2022) and therefore, high microzooplankton biovolume could potentially affect $\varepsilon^2_{Lipid1/Lipid2}$ values.

On a biweekly scale, mean values of modeled $\varepsilon^2_{Lipid1/Lipid2\ phyto}$ and $\varepsilon^2_{Lipid1/Lipid2\ phyto\&zoo}$ values were similar to each other for most sampling dates (Fig. 6). Larger differences were found during peaks of microzooplankton biovolume, and were most pronounced for modeled $\varepsilon^2_{C16:0/phytol}$ and $\varepsilon^2_{sterol/phytol}$ values. For instance, mean $\varepsilon^2_{sterol/phytol\ phyto\&zoo}$ values were > 40 ‰ higher than mean $\varepsilon^2_{sterol/phytol\ phyto}$ values during Ciliata and Rotifera peaks in late October and November.

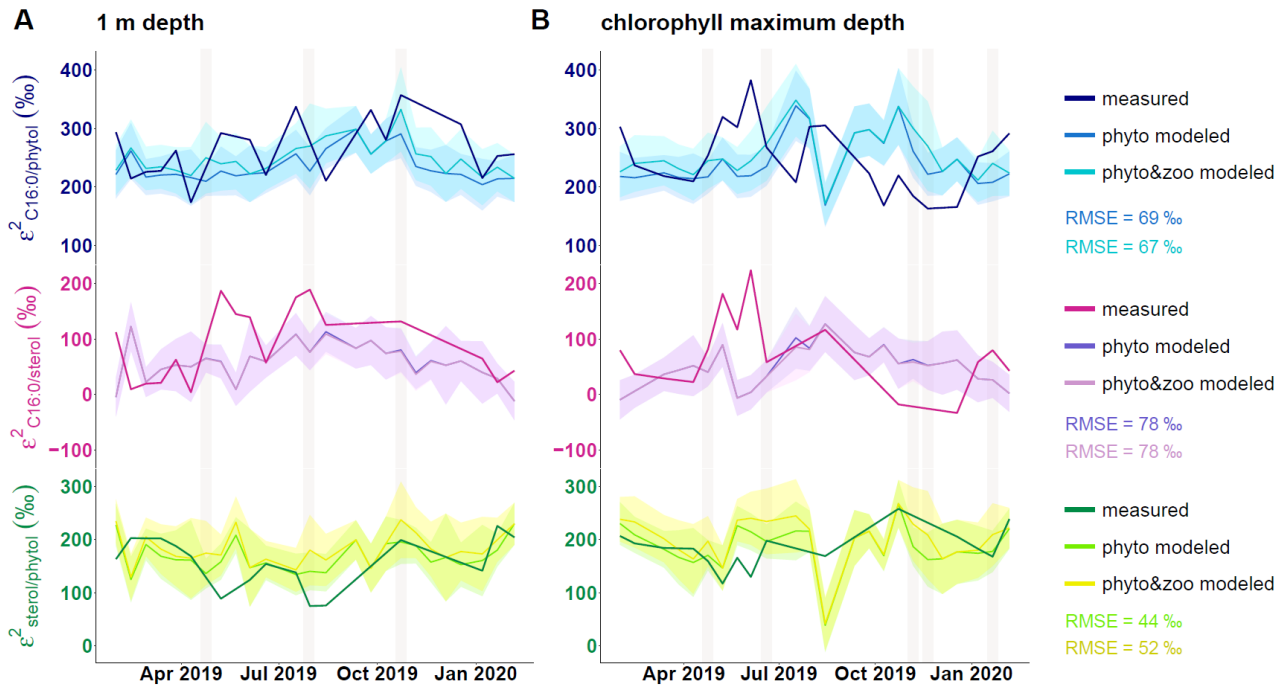

Figure 6: Biweekly comparison of modeled and measured $\varepsilon^2_{Lipid1/Lipid2}$ values in Rotsee at 1 m depth (A) and chlorophyll maximum depth (B). Modeled $\varepsilon^2_{Lipid1/Lipid2}$ values were calculated incorporating weighted $^2H/^1H_{lipid}$ values of autotrophic phytoplankton only ($\varepsilon^2_{Lipid1/Lipid2\ phyto}$) and a combination of weighted $^2H/^1H_{lipid}$ values from autotrophic phytoplankton and heterotrophic microzooplankton ($\varepsilon^2_{Lipid1/Lipid2\ phyto\&zoo}$). For each sampling date, the mean value of modeled $\varepsilon^2_{Lipid1/Lipid2}$ values is shown with the respective standard deviation indicated by shaded areas. Root Mean Square Errors (RMSE) were calculated between measured $\varepsilon^2_{Lipid1/Lipid2}$ values and the mean of modeled $\varepsilon^2_{Lipid1/Lipid2}$ values for each sampling date at both depths. Vertical shaded areas represent microzooplankton biovolume peaks (> 50 % of total biovolume).

Measured $\varepsilon^2_{Lipid1/Lipid2}$ values were nearly identical to the mean of modeled $\varepsilon^2_{Lipid1/Lipid2}$ values on several sampling dates and mostly fell within 1 SD interval. However, larger deviations between measured and modeled $\varepsilon^2_{Lipid1/Lipid2}$ values were found on single sampling dates for all lipid pairs, particularly in early June, when lipids and phytoplankton cells were sampled on different days. Further discrepancies were found in May, when measured $\varepsilon^2_{C16:0/sterol}$ values exceeded the SD interval of modeled $\varepsilon^2_{C16:0/sterol}$ values by nearly 100 ‰ (Fig. 6A), and in mid-August, when measured $\varepsilon^2_{sterol/phytol}$ values were nearly 80 ‰ higher than the SD interval of modeled values (Fig. 6B).

3.5 Yearly and seasonal relationships between $\varepsilon^2_{Lipid1/Lipid2}$ values and phytoplankton community composition

To analyze whether $\varepsilon^2_{Lipid1/Lipid2}$ values on a long-term scale reflect phytoplankton communities and microzooplankton contribution, yearly and seasonal $\varepsilon^2_{Lipid1/Lipid2\ phyto}$ and $\varepsilon^2_{Lipid1/Lipid2\ phyto\&zoo}$ values were modeled and compared to measured amount-weighted average $\varepsilon^2_{Lipid1/Lipid2}$ values (Fig. 7).

Annual and seasonal $\varepsilon^2_{Lipid1/Lipid2\ phyto}$ and $\varepsilon^2_{Lipid1/Lipid2\ phyto\&zoo}$ values were significantly different from each other for all lipid pairs (paired two-sided t-test; $p < 0.0001$), even though the size of this effect was generally small (Fig. 7). On the annual scale, the means of $\varepsilon^2_{C16:0/sterol}$ values were nearly identical between models (Fig. 7B), while for $\varepsilon^2_{C16:0/phytol}$ and $\varepsilon^2_{sterol/phytol}$ values, $\varepsilon^2_{Lipid1/Lipid2\ phyto\&zoo}$ values were ~ 15 and 17 ‰ higher than $\varepsilon^2_{Lipid1/Lipid2\ phyto}$ values (Fig. 7A, C). Seasonally, $\varepsilon^2_{sterol/phytol}$ values displayed the largest difference between models, with mean $\varepsilon^2_{sterol/phytol\ phyto\&zoo}$ values being up to ~ 23 ‰ higher than $\varepsilon^2_{sterol/phytol\ phyto}$ values (Fig. 7C).

On the annual scale, measured $\varepsilon^2_{Lipid1/Lipid2}$ values fell within 1 SD interval of modeled $\varepsilon^2_{Lipid1/Lipid2}$ values for all lipid pairs (Fig. 7), but measured $\varepsilon^2_{C16:0/phytol}$ and $\varepsilon_{sterol/phytol}$ values were > 20 and > 30 ‰ lower than the mean of modeled $\varepsilon^2_{Lipid1/Lipid2\ phyto\&zoo}$ values (Fig. 7A, C). Measured $\varepsilon^2_{Lipid1/Lipid2}$ values were also within 1 SD of modeled values for most lipid pairs in most seasons (Fig. 7). However, there were some discrepancies between measured and modeled $\varepsilon^2_{Lipid1/Lipid2}$ values on the seasonal scale, particularly in autumn.

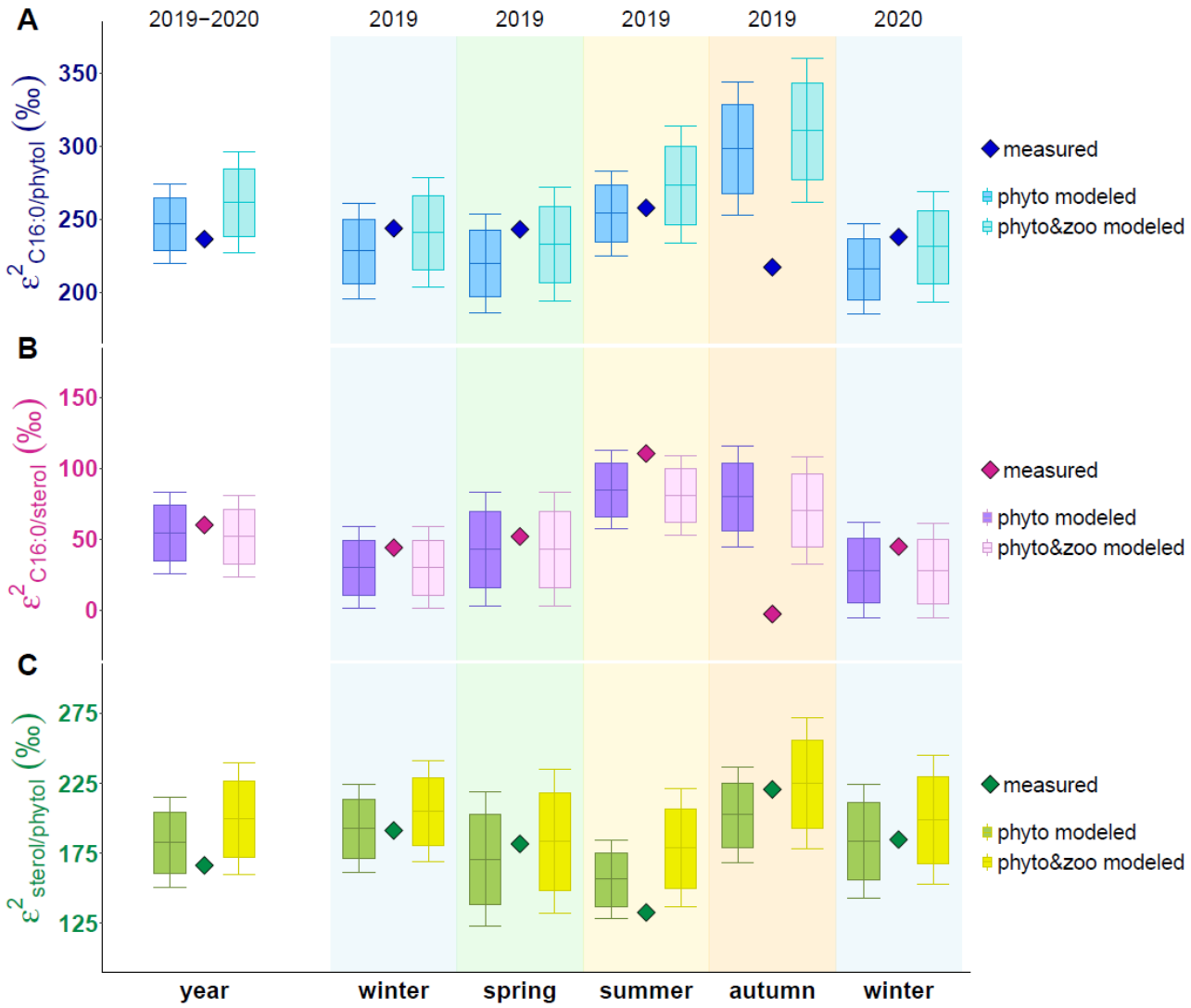

530

531 **Figure 7:** Comparison of modeled and measured weighted average $\varepsilon^2_{Lipid1/Lipid2}$ values in Rotsee over the year
532 (2019-2020) and during meteorological seasons. Modeled $\varepsilon^2_{Lipid1/Lipid2}$ values were calculated incorporating
533 weighted $^2H/^1H_{lipid}$ values of autotrophic phytoplankton only ($\varepsilon^2_{Lipid1/Lipid2\ phyto}$) and a combination of weighted
534 $^2H/^1H_{lipid}$ values from autotrophic phytoplankton and heterotrophic microzooplankton ($\varepsilon^2_{Lipid1/Lipid2\ phyto\&zoo}$). Boxplots
535 indicate the mean of modeled $\varepsilon^2_{Lipid1/Lipid2}$ values with the respective standard deviation. Single rows indicate
536 yearly and seasonal modeled and measured $\varepsilon^2_{C16:0/phytol}$ (A), $\varepsilon^2_{C16:0/sterol}$ (B), and $\varepsilon^2_{sterol/phytol}$ values (C).

537

538 3.6 Phytol:sterol ratios and C18:C16 ratios correlate with
539 cyanobacterial biovolume

540 Alcohols included phytol, diplopterol (hopan-22-ol), brassicasterol, cholesterol (cholest-5-
541 en-3β-ol), ergosterol (methylcholesta-5,7,22-trien-3β-ol), sitosterol, and stigmasterol (Fig.

S4). Cholesterol was excluded from further analysis due to its common abundance in zooplankton (e.g., Goad 1981; Serrazanetti *et al.*, 1992; Wittenborn et al., 2020). The acid fractions contained different saturated and unsaturated fatty acids including C14:0, C16:0, C16:1, C18:0, C18:1, C18:x, C18:2, C18:3nx, C20:3nx, C20:4, C22:2 and C22:6 (Fig. S5). C22:2 was excluded from analysis due to its low abundance at only one sampling date (Fig. S6).

To analyze (dis-)similarities of lipid distributions among samples in relation to phytoplankton community changes, NMDS of relative alcohol concentrations and relative fatty acid concentrations was performed, with visualization of relative cyanobacterial biovolume at each sampling date (Fig. S9). There was a clear separation of samples with high sterol concentrations from samples with high phytol concentrations along NMDS axis 1 (Fig. S9A), with the highest phytol concentrations co-occurring with cyanobacterial blooms. In the analysis of fatty acid abundance, saturated compounds were separated from unsaturated fatty acids along NMDS axis 1 (Fig. S9B). Cyanobacterial blooms co-occurred with high concentrations of C16:1, C18:1, and C20:3nx, and rather high concentrations of C18:2, C18:3nx, and C18:x.

Following NMDS analyses (Fig. S9), we calculated phytol:sterol ratios and C18:C16 ratios (eq. 1 & 2) in the water column of Rotsee and analyzed their relationship with cyanobacterial biovolume (Fig. 8).

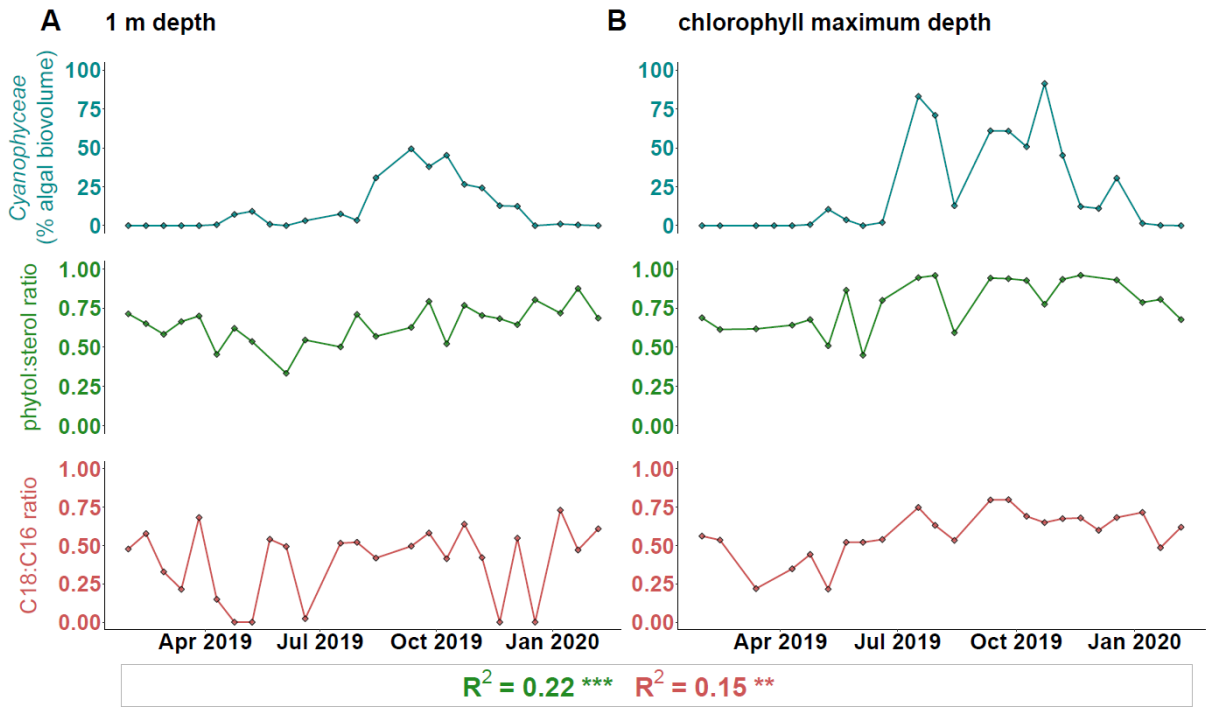

561

562 **Figure 8:** Time series of relative cyanobacterial biovolume, phytol:sterol ratios and C18:C16 ratios in Rotsee
563 at 1 m depth (A) and chlorophyll maximum depth (B). R^2 values refer to linear regressions between phytol:sterol
564 ratios and cyanobacterial biovolume, as well as C18:C16 ratios and cyanobacterial biovolume analyzed for
565 combined sampling depths. **: P < 0.01; ***: P < 0.001.

566 At 1 m depth, cyanobacteria were generally not abundant, with the exception of a bloom
567 in September and October, where cyanobacterial biovolume increased to > 40 % of total
568 phytoplankton biovolume (Fig. 3; Fig. 8). During cyanobacterial blooms, phytol:sterol ratios
569 and C18:C16 ratios increased to > 0.5. At the chlorophyll maximum depth, cyanobacterial
570 blooms occurred in July and in September/October, with cyanobacterial biovolume
571 increasing to > 60 % and > 90 % of total algal biovolume (Fig. 3; Fig. 8). Phytol:sterol ratios
572 clearly increased during cyanobacterial blooms to > 0.9. C18:C16 also increased but to a
573 lesser extent, with a maximum of ~ 0.6 in late September (Fig. 8B). Cyanobacterial
574 biovolume was significantly positively correlated with both lipid ratios.

575

4. Discussion

We analyzed $\varepsilon^2_{Lipid1/Lipid2}$ values and the distribution of algal lipids in the water column of Rotsee in relation to phytoplankton community changes throughout a one-year sampling period. δ^2H_{lipid} values had much greater variability than δ^2H_{water} values (Fig. 4), suggesting that other factors besides δ^2H_{water} values, such as the composition of the algal community, are more important in determining δ^2H_{lipid} values. However, algal δ^2H_{lipid} values could still be used as a proxy for δ^2H values of lake water as changes in the phytoplankton community could be disentangled from changes in past δ^2H_{water} values by the comparison of δ^2H values of source-specific and generic lipids as suggested by Ladd *et al.* (2024).

In the following discussion, we evaluate hydrogen isotope offsets among lipids, specifically $\varepsilon^2_{C16:0/phytol}$, $\varepsilon^2_{C16:0/sterol}$, and $\varepsilon^2_{sterol/phytol}$ values, as potential indicators for phytoplankton community dynamics and lipid ratios as proxy for cyanobacterial biovolume. We discuss uncertainties in their interpretation and further consider their application in paleoecological contexts to reconstruct past phytoplankton community dynamics.

4.1 Evaluation of $\varepsilon^2_{Lipid1/Lipid2}$ values as indicators of phytoplankton community compositions

Relationships between biweekly $\varepsilon^2_{Lipid1/Lipid2}$ values and algal biovolume in Rotsee (Fig. S5, S6) were generally in accordance with previous culturing studies (Ladd *et al.,* 2024). During the cyanobacterial bloom in summer (Fig. 3B), $\varepsilon^2_{C16:0/phytol}$ values increased up to 302 ‰, consistent with high $\varepsilon^2_{C16:0/phytol}$ values from cyanobacterial cultures (351 +/- 99 ‰; Ladd *et al.,* 2024). Likewise, diatom blooms were associated with high $\varepsilon^2_{sterol/phytol}$ values (> 200 ‰) and low $\varepsilon^2_{C16:0/sterol}$ values (< 100 ‰), similar to diatom cultures (248 +/- 45 ‰ and -25 +/- 49 ‰; Ladd *et al.,* 2024). Therefore, $\varepsilon^2_{Lipid1/Lipid2}$ values might be indicative for specific algal groups if they form a dominant part within the phytoplankton community. Additionally, changes in $\varepsilon^2_{C16:0/sterol}$ and $\varepsilon^2_{sterol/phytol}$ values might indicate shifts within the eukaryotic algal community,

even if groups with similar $\varepsilon^2_{Lipid1/Lipid2}$ values, such as diatoms and golden algae, cannot be resolved from each other (Fig. 5).

In contrast to expectations from algal cultures (Ladd *et al.,* 2024), there was no relationship between $\varepsilon^2_{C16:0/phytol}$ values and the summed biovolume of cyanobacteria and green algae (Fig. S5). This lack of relationship may be partly due to the overlap of the main cyanobacterial bloom in late October (> 90 % of algal biovolume (Fig. 3B)) with the initiation of the autumnal mixing (Fig. 2), potentially transferring organic matter from the deeper hypolimnion to the epilimnion. Lipid concentrations and δ^2H_{lipid} values in our study were probably biased by the lake turnover event, which could also account for the large deviation between measured and modeled $\varepsilon^2_{C16:0/phytol}$ and $\varepsilon^2_{sterol/phytol}$ values in autumn (Fig. 7). The complete mixing of the water column in winter (Fig. 2) could further contribute to the discrepancies between measured and modeled $\varepsilon^2_{C16:0/phytol}$ and $\varepsilon^2_{C16:0/sterol}$ values on the biweekly scale (Fig.6), which were less pronounced in weighted-average $\varepsilon^2_{Lipid1/Lipid2}$ values in winter (Fig. 7). The impact of the mixing event was also seen for phytol:sterol ratios, which had stronger correlations with cyanobacterial biovolume when sampling dates during lake mixing were excluded (2019-10-09 to 2019-12-04) ($R^2 = 0.27$, $p < 0.001$).

Additionally, increasing cellular growth rates during the cyanobacterial bloom could impact $\varepsilon^2_{C16:0/phytol}$ values, since higher growth rates have been shown to cause ^2H depletion in lipids of some eukaryotic algae, likely due to higher contributions of ^2H-deleted NADPH from photosystem I (PS I) (e.g., Z. Zhang *et al.,* 2009; Sachs & Kawka 2015). However, differences between algal groups and lipids exist. While various lipids of *Emiliania huxleyi* became ^2H-deleted, fatty acids of *Thalassiosira pseudonana* have been found to be unaffected by higher cellular growth rates (Z. Zhang *et al.,* 2009; Sachs & Kawka 2015). Likewise, the measured $\delta^2H_{C16:0}$ value (-267 ‰) during the cyanobacterial bloom was within expectations from cyanobacterial batch cultures (-236 +/- 32 ‰; Ladd *et al.*, 2024). The δ^2H_{phytol} value (-399 ‰) was, however, more ^2H-enriched than expected (-433 +/- 18 ‰; Ladd *et al.*, 2024) contradicting the expected growth rate effect on lipid hydrogen isotope fractionation.

A more likely explanation for the ^{2}H-enrichement of phytol could be the abundance of cyanobacterial species with rather high $\delta^{2}H_{phytol}$ values as there is a high intraspecies variability within algal groups (Ladd *et al.,* 2024). Unfortunately, the main cyanobacteria contributing to the bloom event could only be assigned to the order Chroococcales, with no further species identification. Future culturing studies comprising more cyanobacteria species are needed to better constrain the range of cyanobacterial $\delta^{2}H_{phytol}$ values.

Moreover, mixotrophic growth of cyanobacteria due to light limitation by self-shading effects, as well as decreasing CO_2 concentrations during the bloom event could potentially cause ^{2}H-enrichement of phytol (Zagarese *et al.,* 2021; Cormier *et al.,* 2022; Muñoz-Marín *et al.,* 2024; Torres-Romero *et al.,* 2024). During algal mixotrophy, the higher relative proportion of ^{2}H-enriched NADPH from glycolysis or the oxidative pentose phosphate pathway (oxPPP) causes a ^{2}H-enrichement during lipids synthesis (Cormier *et al.,* 2022). The potential impact of mixotrophic growth on $\varepsilon^{2}_{Lipid1/Lipid2}$ values was further indicated by large discrepancies between measured and modeled $\varepsilon^{2}_{Lipid1/Lipid2}$ values during a dinoflagellate bloom in mid-August (Fig. 3B; Fig. 6B), which mainly consisted of the mixotrophic species *Ceratium hirundinella* (e.g., Callieri et al., 2006).

Generally, mixotrophy dominates in oligotrophic lakes and during low light and low nutrient availability (Caron *et al.,* 1993; Pålsson & Granéli 2004; Saad *et al.,* 2016). Therefore, although mixotrophy in Rotsee might be reflected in single $\varepsilon^{2}_{Lipid1/Lipid2}$ values, the general mixotrophic impact on $\varepsilon^{2}_{Lipid1/Lipid2}$ values in eutrophic lake systems is probably low, especially over longer timescales.

In addition to phytoplankton groups in Rotsee, heterotrophic microzooplankton represent another lipid source (Fig. 3), potentially impacting $\varepsilon^{2}_{Lipid1/Lipid2}$ values. $\delta^{2}H_{lipid}$ values of heterotrophic organisms are expected to be higher than algal $\delta^{2}H_{lipid}$ values as NAD(P)H derived from glycolysis or oxPPP is ^{2}H-enriched compared to the extremely ^{2}H-depleted NADPH formed in photosystem I (PS I) of phototrophs (e.g., Schmidt *et al*., 2003; X. Zhang *et al.* 2009; Cormier *et al.*, 2018; Cormier *et al.,* 2022). To assess the potential isotopic impact of microzooplankton peaks on $\varepsilon^{2}_{Lipid1/Lipid2}$ values, we modeled $\varepsilon^{2}_{Lipid1/Lipid2\ phyto}$ and

658 $\varepsilon^2_{\text{Lipid1/Lipid2 phyto\&zoo}}$ values and compared modeling results with measured $\varepsilon^2_{\text{Lipid1/Lipid2}}$ values
659 (Fig. 6, 7). While $\varepsilon^2_{\text{Lipid1/Lipid2 phyto}}$ values solely incorporate biovolume-weighted δ^2H_{lipid} values
660 of phytoplankton groups derived from batch cultures (Ladd *et al*., 2024), $\varepsilon^2_{\text{Lipid1/Lipid2 phyto\&zoo}}$
661 values additionally include theoretical $\delta^2H_{C16:0}$ and $\delta^2H_{\text{sterol}}$ values of heterotrophs weighted by
662 microzooplankton biovolume. Beside the contributions of H from different NAD(P)H pools,
663 lipid hydrogen isotope fractionation in heterotrophs further depends on dietary and water δ^2H
664 values, as well as kinetic fractionation by enzymes during fatty acid synthesis (Solomon *et*
665 *al.,* 2009; X. Zhang *et al.,* 2009; Vander Zanden *et al.,* 2016; Pilecky *et al*., 2022). We
666 accounted for the net impact of these different processes by the application of an empirically
667 derived fractionation factor between $\delta^2H_{C16:0}$ values of seston and zooplankton (Pilecky *et al.,*
668 2022). This might overestimate the isotope fractionation between algal and heterotrophic
669 $\delta^2H_{\text{sterol}}$ values, as microzooplankton might simply assimilate algal sterols, but the synthesis
670 of phytosterols by microzooplankton cannot be excluded (Boëchat *et al.*, 2007; Michellod *et*
671 *al.,* 2023). Additional uncertainty in our modeled $\varepsilon^2_{\text{Lipid1/Lipid2}}$ values comes from the relatively
672 small number of freshwater taxa from which culturing data are available (Ladd *et al.*, 2024).

673 Despite the large uncertainties, measured $\varepsilon^2_{\text{Lipid1/Lipid2}}$ values were nearly identical to the
674 mean of modeled algal $\varepsilon^2_{\text{Lipid1/Lipid2 phyto}}$ values on multiple sampling dates (Fig. 6), indicating
675 that phytoplankton community composition is reflected by $\varepsilon^2_{\text{Lipid1/Lipid2}}$ values. Although several
676 microzooplankton peaks occurred throughout the year (Fig. 3), the RMSE of modeled
677 $\varepsilon^2_{\text{Lipid1/Lipid2 phyto}}$ and $\varepsilon^2_{\text{Lipid1/Lipid2 phyto\&zoo}}$ values were mostly similar (Fig. 6A, B), supporting a
678 generally minor isotopic impact of microzooplankton. This is in accordance with short-term
679 ^{13}C-labelling experiments suggesting that Rotsee is net autotrophic (Lammers *et al.,* 2016).
680 Large discrepancies between measured and modeled $\varepsilon^2_{\text{Lipid1/Lipid2 phyto}}$ values can be partly
681 explained by mixotrophy of phytoplankton (see above) as well as the uncertainty associated
682 with δ^2H_{lipid} values modeled for cryptomonads. The various *Cryptomonas* species in Rotsee
683 might be poorly represented by δ^2H_{lipid} values from batch cultures, which included only
684 *Cryptomonas ovata* (Ladd *et al.,* 2024). When measured $\varepsilon^2_{\text{C16:0/sterol}}$ values exceeded the

modeled SD interval by nearly 80 ‰ in early May, cryptomonads comprised 70 % of eukaryotic algal biovolume, emphasizing the need for further culturing studies.

4.2 Lipid ratios as proxies for cyanobacterial biovolume

Besides $\varepsilon^2_{Lipid1/Lipid2}$ values, we investigated lipid distributions in the water column in relation to phytoplankton biovolume. Phytol:sterol ratios were positively correlated with cyanobacterial biovolume (R^2= 0.22; $p < 0.001$) (Fig. S9, Fig. 8), in accordance with previous findings that most cyanobacteria do not produce any sterols (Martin-Creuzburg *et al.,* 2008; Taipale *et al.,* 2016; Peltomaa *et al.,* 2023). The co-occurrence of unsaturated C18 fatty acids with high cyanobacterial biovolume in Rotsee is consistent with the use of unsaturated C18 fatty acids as cyanobacterial biomarker (Bauersachs *et al*., 2017; Zeman-Kuhnert *et al.,*2023). However, high concentrations of polyunsaturated C18 fatty acids have also been found in different green algae, as well as Chromalveolates (Taipale *et al.,* 2016; Lang *et al.,* 2011) and some cyanobacteria strains produce similar amounts of C16:0 and C18:3ω3 (Peltomaa *et al.,* 2023). Therefore, the separation of eukaryotic algae and cyanobacteria by C18:C16 ratios is probably less strict than by phytol:sterol ratios, which is also indicated by the weaker correlation between C18:C16 ratios and cyanobacterial biovolume (R^2= 0.15; $p < 0.01$) (Fig. 8).

In general, phytol:sterol ratios and C18:C16 ratios might also be impacted by changes in temperature, phosphorus and silicate availability which affect algal sterol and fatty acid production rates (Piepho *et al.,* 2010; Piepho *et al.,* 2012; Matsui *et al.,* 2020; Calderini *et al.,* 2023). In Rotsee, water temperatures at different sampling depths ranged from 4 to 25 °C and phosphorus concentrations ranged from 8 to 56 µg/L throughout the year. Only absolute concentrations of brassicasterol ($R^2 = 0.14$, $p < 0.01$) and C20:4 fatty acid ($R^2 = 0.07$, $p < 0.05$) (µg/L) were significantly negatively correlated with temperature, suggesting a rather minor impact of temperature on lipid synthesis or no general trend among different phytoplankton species as proposed by Piepho *et al.* (2012). However, concentrations of

C16:1 (R^2 = 0.2, $p < 0.001$), C18:2 (R^2 = 0.1, $p < 0.05$), C18:x (R^2 = 0.1, $p < 0.05$) and C18:1 (R^2 = 0.1, $p < 0.05$) were significantly positively correlated with total phosphorus concentrations as well as phytol:sterol ratios (R^2 = 0.28, $p < 0.001$) and C18:C16 ratios (R^2 = 0.12, $p < 0.01$). Phytoplankton growth in eutrophic lakes is generally limited by phosphorus (e.g., Liang et al., 2020; Jiang & Nakano 2022), and increasing phosphorus concentrations can potentially promote cyanobacterial blooms (e.g., Huisman *et al*., 2018; Jankowiak *et al.*, 2019). Although there was a collinearity between phosphorus, nitrogen and temperature, relative cyanobacterial biovolume in Rotsee was positively associated with high phosphorus concentrations (Fig. S10). Therefore, the significant correlation between lipid ratios and total phosphorus concentrations is likely an indirect effect resulting from phosphorus fertilization of cyanobacteria.

4.3 $\varepsilon^2_{Lipid1/Lipid2}$ values and lipid ratios as paleoecological proxies for phytoplankton community dynamics

Annually-integrated and amount-weighted $\varepsilon^2_{Lipid1/Lipid2}$ values are likely the most representative of a potential sedimentary isotopic signal, as sediment samples typically incorporate longer timescales, with an average sedimentation rate of 0.38 cm yr^{-1} in Rotsee (Naeher *et al.*, 2012). Annual $\varepsilon^2_{Lipid1/Lipid2}$ values based on water column measurements were almost identical to modeled algal $\varepsilon^2_{Lipid1/Lipid2\ phyto}$ values (Fig. 7) and did not reflect the short-term impact of the lake mixing event and signatures of heterotrophic and/or mixotrophic δ^2H_{lipid} values. Therefore, long-term $\varepsilon^2_{Lipid1/Lipid2}$ values in the water column of eutrophic lakes like Rotsee are expected to mainly reflect phytoplankton community compositions, especially as the δ^2H values of carbon-bound hydrogen are stable during early diagenesis (Schimmelmann *et al.,* 2006).

However, lipid degradation during the transfer from the water column to the sediment might complicate the interpretation of sedimentary $\varepsilon^2_{Lipid1/Lipid2}$ values and lipid ratios. Degradation susceptibilities vary among algal lipids (e.g., Kawamura *et al.,* 1987; Rontani &

739 Volkman 2003; Martin-Creuzberg & von Elert 2004; Peltomaa *et al*., 2017; Zeman-Kuhnert *et*
740 *al.,* 2023), and can lead to ^{2}H-enrichment of lipids in surface sediment relative to the water
741 column (e.g. Gray *et al.,* 2002; Mancini *et al*., 2003; Miljević & Golobočanin 2007; Sachs &
742 Schwab, 2011; Schwab et al., 2015; Ladd *et al*., 2018) or to changes in the relative
743 abundance of different compounds. In particular, the relatively fast mineralization of
744 polyunsaturated C18 fatty acids compared to saturated fatty acids like C16:0 (Kawamura *et*
745 *al.,* 1987) likely compromises the significance of C18:C16 ratios as a paleoecological proxy.
746 The phytol:sterol ratio could likely be adapted to longer timescales by including degration
747 products of phytol (e.g. pristane, isomeric pristenes, phytadienes, phytenic acid and
748 phytenes; Jeng *et al.,* 1997; Grossi *et al*., 1998; Rontani *et al*., 1999; Rontani & Volkman
749 2003) and sterols (stanols; Killops & Killops 2004; Brocks *et al.,* 2017; Brocks *et al.,* 2023).

750 In addition to degradation, sedimentary $\delta^{2}H$ values and lipid ratios could also be affected
751 by non-algal sources of organic matter, including microbes, macrophytes, and larger
752 mesoplankton. In eutrophic lakes like Rotsee, however, algal contributions likely dominate
753 microbial fatty acid inputs (Heinzelmann *et al.,* 2018). Likewise, larger mesoplankton typically
754 comprise only ~ 1 to 5 % of phytoplankton biomass in eutrophic lakes (Yuan & Pollard 2018).
755 Beside autochthonous sources, organic input from the catchment vegetation (Bloesch 1974)
756 could transfer plant lipids to the sediment. However, due to their location in cell membranes
757 and the plastid (Rustan & Drevon 2005; Dufourc 2008; Anderson 1975), C16:0 fatty acid,
758 sterols and phytol have a less direct transit pathway to lake waters compared to leaf waxes
759 which are abraded from surface cuticular layers by wind (Nelson *et al.,* 2018).

760 Despite these potential complications, sedimentary $\varepsilon^{2}_{Lipid1/Lipid2}$ values and lipid ratios are a
761 promising tool to increase the robustness of phytoplankton community reconstructions.
762 Specifically, downcore $\varepsilon^{2}_{C16:0/sterol}$ and $\varepsilon^{2}_{sterol/phytol}$ values could trace past shifts in the
763 eukaryotic algal community, with high $\varepsilon^{2}_{sterol/phytol}$ values (> 200 ‰) and low $\varepsilon^{2}_{C16:0/sterol}$ values
764 (< 100 ‰) being indicative for a dominance of diatoms and/or golden algae (Fig. 5, Fig. 9).
765 Moreover, a co-occurrence of high $\varepsilon^{2}_{C16:0/phytol}$ values (> 250 ‰) and high phytol:sterol ratios

(> 0.75) can be expected during phases of high cyanobacterial and rather low eukaryotic algal biomass (Fig. 9).

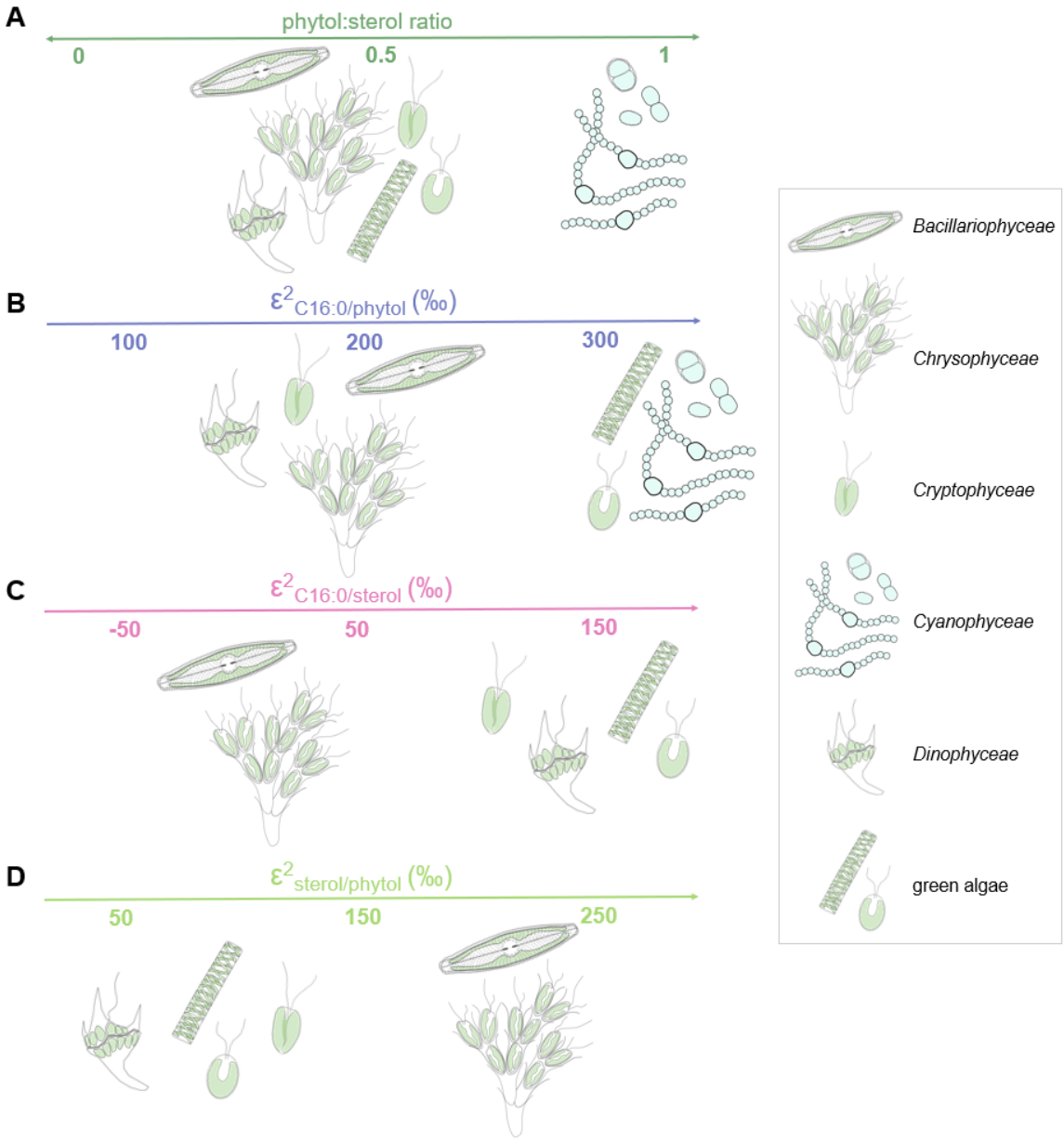

Figure 9: Schematic illustration of how phytol:sterol ratios (A), $\varepsilon^2_{C16:0/phytol}$ (B), $\varepsilon^2_{C16:0/sterol}$ (C), and $\varepsilon^2_{sterol/phytol}$ (D) values could be used as proxies for phytoplankton community composition.

Additionally, the combination of $\varepsilon^2_{Lipid1/Lipid2}$ values and lipid ratios with proxies for individual algal groups offers the opportunity to analyze past relationships between single algal groups and the phytoplankton community. For instance, while diatom abundance and

775 species richness can be quantitatively inferred by their silica frustules, the additional analysis
776 of $\varepsilon^2_{C16:0/sterol}$ and $\varepsilon^2_{sterol/phytol}$ values would indicate if diatoms were dominant within the
777 phytoplankton community. The proportion of golden algae and diatoms could be further
778 disentangled by the ratio of diatom frustules and statospores of golden algae species (Smol
779 1985). Recently, *sed*aDNA approaches have been widely used to reconstruct past
780 cyanobacterial dynamics, also in combination with other algal proxies, e.g. sedimentary
781 pigments (e.g., Pal *et al.,* 2015; Cao *et al.*, 2020; Nwosu *et al*., 2023). The application of
782 *sed*aDNA together with $\varepsilon^2_{C16:0/phytol}$ values and phytol:sterol ratios would reveal not only past
783 cyanobacterial abundance, but also their relative abundance to eukaryotic algae.

784 Moreover, due to their good preservation, sedimentary $\varepsilon^2_{C16:0/phytol}$ values and phytol:sterol
785 ratios, including phytol and sterol degradation products, might be an alternative approach to
786 reconstruct past cyanobacterial dynamics over geologic timescales. The potential short-term
787 influence of environmental variables on eukaryotic algal sterol contents (Piepho *et al.,* 2010;
788 Piepho *et al.,* 2012) is likely averaged out, especially when analyzing distinct time periods
789 with relatively constant temperature and nutrient supply. Several paleoecological studies
790 have already used the increasing abundance of sterols in the geologic record as proxy for
791 the rising appearance of eukaryotic algae (Brocks *et al.,* 2017; Brocks *et al.,* 2023).
792 Phytol:sterol ratios in the sediment might, however, still be biased by the differences in sterol
793 content among eukaryotic algal species (e.g, Martin-Creuzburg & Merkel 2016; Volkman
794 2003; Rampen *et al.,* 2010; Taipale *et al.,* 2016). To minimize the impact of species
795 variability, we propose phytol:sterol ratios of > 0.75 as an indicator of cyanobacterial
796 dominance, representing values recorded in Rotsee during cyanobacterial blooms (Fig. 8B).
797 Moreover, to increase the robustness of phytol:sterol ratios, we suggest excluding sterols
798 potentially produced by sedimentary fungi, e.g., ergosterol or fungisterol (Weete 1989;
799 Gessner & Chauvet 1993; Volkman 2003).

800

5. Conclusions

Biweekly measurements of algal lipid distributions and $\varepsilon^2_{C16:0/phytol}$, $\varepsilon^2_{C16:0/sterol}$, and $\varepsilon^2_{sterol/phytol}$ values in the water column of Rotsee were related to phytoplankton community composition over a one-year sampling period.

The summed biovolume of diatoms and golden algae was positively correlated with $\varepsilon^2_{sterol/phytol}$ values and negatively correlated with $\varepsilon^2_{C16:0/sterol}$ values, while the remaining eukaryotic algal groups had the opposite relationships. Comparing measured $\varepsilon^2_{Lipid1/Lipid2}$ values and modeled $\varepsilon^2_{Lipid1/Lipid2}$ values incorporating multiple lipid end-members indicated that heterotrophic microzooplankton and mixotrophy may affect $\varepsilon^2_{Lipid1/Lipid2}$ values on short time-scales, but that long-term $\varepsilon^2_{Lipid1/Lipid2}$ values in the water column of eutrophic lake systems generally reflect the phytoplankton community composition. The analysis of algal lipid distributions indicated increasing concentrations of phytol and unsaturated C18 fatty acid during cyanobacterial blooms, and phytol:sterol ratios and C18:C16 ratios were significantly positively correlated with cyanobacterial biovolume. Due to the good preservation of lipids in sediment, particularly phytol:sterol ratios, combined with $\varepsilon^2_{C16:0/phytol}$ values, provide a promising tool for the reconstruction of past cyanobacterial blooms.

Generally, the interpretation of sedimentary $\varepsilon^2_{Lipid1/Lipid2}$ values and lipid ratios should consider the trophic status of the lacustrine system. In eutrophic lakes like Rotsee, phytoplankton are the main lipid source, likely overwhelming the isotopic imprint and lipid contribution of other autochthonous origins to the sediment. In oligotrophic lake systems, however, the relative importance of other aquatic lipid producers might be higher, and $\varepsilon^2_{Lipid1/Lipid2}$ values could be further impacted by a higher proportion of phytoplankton mixotrophy. We therefore emphasize the interpretation of sedimentary $\varepsilon^2_{Lipid1/Lipid2}$ values and lipid ratios in a multi-proxy context integrating complementary lines of evidence.

Acknowledgements

This research was funded by a Swiss National Science Foundation (SNSF) Eccellenza Fellowship to SNL (PCEFP2 194211), an SNSF Prima Fellowship to CDJ (179783), and Eawag internal funds. Patrick Kathriner, Karin Beck, Nina Studhalter, Sandra Schmid, and Alois Zwyssig assisted with the field work. Argton Zeqiri and Serge Robert assisted with lipid extractions and alcohol analyses. Patrick Kathriner assisted with the preparation of water samples for nutrient analyses. Nitrogen and phosphorus concentrations were measured at the Eawag AuA laboratory.

Appendix A. Supplementary Material

Supplemental figures S1 – S10 are included as an online appendix to this manuscript.

Author contributions

Conceptualization: AK, SNL, DBN, ND, CJS; Formal analysis: AK; Funding acquisition: SNL, CDJ, CJS; Investigation: AK, SNL, DBN, CDJ, MR; Methodology: AK, SNL, DBN, MR; Project administration: SNL, CDJ, ND, CJS; Supervision: SNL; Visualization: AK; Writing – original draft: AK; Writing - review & editing: All

Data availability

All data are available through the Dryad Digital Repository (https://doi.org/10.5061/dryad.9s4mw6mrm). All R scripts and related data files are uploaded in GitHub (https://github.com/antoniaKlatt/Klatt_etal_2024_phytoplankton_Rotsee).

References

Acevedo-Trejos, E., Brandt, G., Bruggeman, J., Merico, A., 2015: Mechanisms shaping size structure and functional diversity of phytoplankton communities in the ocean. Sci. Rep. 5, 8918.

Anderson, J.M., 1975: Possible location of chlorophyll within chloroplast membranes. Nature 253, 536–537.

Arhonditsis, G.B., Stow, C.A., Steinberg, L.J., Kenney, M.A., Lathrop, R.C., McBride, S.J., Reckhow, K.H., 2006: Exploring ecological patterns with structural equation modeling and Bayesian analysis. Ecol. Modell. 192, 385–409.

Baan, J., Holloway-Phillips, M., Nelson, D.B., Kahmen, A., 2023: The metabolic sensitivity of hydrogen isotope fractionation differs between plant compounds. Phytochem. 207, 113563.

Bauersachs, T., Talbot, H.M., Sidgwick, F., Sivonen, K., Schwark, L., 2017: Lipid biomarker signatures as tracers for harmful cyanobacterial blooms in the Baltic Sea. PLoS ONE 12, e0186360.

Bloesch, J., 1974: Sedimentation und Phosphorhaushalt im Vierwaldstättersee (Horwer Bucht) und im Rotsee. Schweiz. Z. Hydrologie 36, 71–186.

Brocks, J.J., Nettersheim, B.J., Adam, P., Schaeffer, P., Jarrett, A.J.M., Güneli, N., Liyanage, T., van Maldegem, L. M., Hallmann, C., Hope, J.M., 2023: Lost world of complex life and the late rise of the eukaryotic crown. Nature 618, 767–773.

Brocks, J.J., Jarrett, A.J.M., Sirantoine, E., Hallmann, C., Hoshino, Y., Liyanage, T., 2017: The rise of algae in Cryogenian oceans and the emergence of animals. Nature 548, 578–581.

Calderini, M.L., Pääkkönen, S., Salmi, P., Peltomaa, E., Taipale, S.J., 2023: Temperature, phosphorus and species composition will all influence phytoplankton production and content of polyunsaturated fatty acids. J. Plankton Res. 45, 625–635.

Callieri, C., Caravati, E., Morabito, G., Oggioni, A., 2006: The unicellular freshwater cyanobacterium *Synechococcus* and mixotrophic flagellates: evidence for a functional association in an oligotrophic, subalpine lake. Freshw. Biol. 51, 263–273.

Callisto, M., Molozzi, J., Barbosa, J.L.E., 2014: Eutrophication of Lakes, in: Ansari, A., Gill, S. (Eds.), Eutrophication: Causes, Consequences and Control. Springer, Dordrecht, pp. 55–71.

Cao, X., Xu, X., Bian, R., Wang, Y., Yu, H., Xu, Y. Duan, G., Bi, L., Chen, P., Gao, S., Wang, J., Peng, J., Qu, J., 2020: Sedimentary ancient DNA metabarcoding delineates the contrastingly temporal change of lake cyanobacterial communities. Water Res. 183, 116077.

Capo, E., Debroas, D., Arnaud, F., Domaizon, I., 2015: Is Planktonic Diversity Well Recorded in Sedimentary DNA? Toward the Reconstruction of Past Protistan Diversity. Microb. Ecol. 70, 865–875.

Capo, E., Monchamp, M.-E., Coolen, M.J.L., Domaizon, I., Armbrecht, L., Bertilsson, S., 2022: Environmental paleomicrobiology: using DNA preserved in aquatic sediments to its full potential. Environ. Microbiol. 24, 2201–2209.

Caron, D.A., Sanders, R.W., Lim, E.L., Marrasé, C., Amaral, L.A., Whitney, S., Aoki, R.B., Porters, K.G., 1993: Light-dependent phagotrophy in the freshwater mixotrophic chrysophyte *Dinobryon cylindricum*. Microb. Ecol. 25, 93–111.

Cormier, M.-A., Berard, J.-B., Bougaran, G., Trueman, C.N., Mayor, D.J., Lampitt, R.S., Kruger, N.J., Flynn, K.J., Rickaby, R.E.M., 2022: Deuterium in marine organic biomarkers: toward a new tool for quantifying aquatic mixotrophy. New Phytol. 234, 776–782.

Cormier, M.-A., Werner, R.A., Sauer, P.E., Gröcke, D.R., Leuenberger, M.C., Wieloch, T., Schleucher, J., Kahmen, A., 2018: ^{2}H-fractionations during the biosynthesis of carbohydrates and lipids imprint a metabolic signal on the δ^{2}H values of plant organic compounds. New Phytol. 218, 479–491.

Cvetkoska, A., Jovanovska, E., Hauffe, T., Donders, T.H., Levkov, Z., van de Waal, D.B., Reed, J.M., Francke, A., Vogel, H., Wilke, T., Wagner, B., Wagner-Cremer, F., 2021: Drivers of phytoplankton community structure change with ecosystem ontogeny during the Quaternary. Quat. Sci. Rev. 265, 107046.

Dale, B., Fjellså, A., 1994: Dinoflagellate Cysts as Paleoproductivity Indicators: State of the Art, Potential, and Limits, in: Zahn, R., Pedersen, T.F., Kaminski, M.A., Labeyrie, L. (Eds.), Carbon Cycling in the Glacial Ocean: Constraints on the Ocean's Role in Global Change. NATO ASI Series 17. Springer, Berlin, Heidelberg, pp. 521–537.

Darling, W.G., Bath, A.H., Gibson, J.J., Kazimierz, R., 2006: Isotopes in water. in: Leng, M.J. (Eds.), Isotopes in Palaeoenvironmental Research. Springer, Dordrecht, pp. 1–66.

Desmond, E., Gribaldo, S., 2009: Phylogenomics of Sterol Synthesis: Insights into the Origin, Evolution, and Diversity of a Key Eukaryotic Feature. Genome Biol. Evol. 1, 364–381.

Dufourc, E.J., 2008: Sterols and membrane dynamics. J. Chem. Biol. 1, 63–77.

Gessner, M.O., Chauvet, E., 1993: Ergosterol-to-Biomass Conversion Factors for Aquatic Hyphomycetes. Appl. Environ. Microbiol. 59, 502–507.

Goad, L.J., 1981: Sterol biosynthesis and metabolism in marine invertebrates. Pure Appl. Chem. 51, 837–852.

Gray, J.R., Lacrampe-Couloume, G., Gandhi, D., Scow, K.M., Wilson, R.D., Mackay, D.M., Sherwood Lollar, B., 2002: Carbon and Hydrogen Isotopic Fractionation during Biodegradation of Methyl tert-Butyl Ether. Environ. Sci. Tech. 36, 1931–1938.

Grossi, V., Hirschler, A., Raphel, D., Rontani, J.-F., Leeuw, J.W. de, Bertrand, J.-C., 1998: Biotransformation pathways of phytol in recent anoxic sediments. Org. Geochem. 29, 845–861.

Harrell Jr. F., 2023: Hmisc: Harrell Miscellaneous. R package version 5.1-0. https://CRAN.R-project.org/package=Hmisc.

Hastie, T., Tibshirani, R., Friedman, J., 2009: The Elements of Statistical Learning, second ed., Springer, New York.

Heinzelmann, S.M., Chivall, D., M'Boule, D., Sinke-Schoen, D., Villanueva, L., Sinninghe Damsté, J.S., Schouten, S., van der Meer, M.T.J., 2015: Comparison of the effect of salinity on the D/H ratio of fatty acids of heterotrophic and photoautotrophic microorganisms. FEMS Microbiol. Lett. 362, fnv065.

Heinzelmann, S.M., Villanueva, L., Lipsewers, Y.A., Sinke-Schoen, D., Sinninghe Damsté, J.S., Schouten, S., van der Meer, M.T.J., 2018: Assessing the metabolism of sedimentary microbial communities using the hydrogen isotopic composition of fatty acids. Org. Geochem.124, 123–132.

Henson, S.A., Cael, B.B., Allen, S.R., Dutkiewicz, S., 2021: Future phytoplankton diversity in a changing climate. Nat. Commun. 12, 5372.

947 Hinder, S.L., Hays, G.C., Edwards, M., Roberts, E.C., Walne, A.W., Gravenor, M.B., 2012:
948 Changes in marine dinoflagellate and diatom abundance under climate change.
949 Nat. Clim. Change 2, 271–275.

950 Hirave, P., Glendell, M., Birkholz, A., Alewell, C., 2021: Compound-specific isotope analysis
951 with nested sampling approach detects spatial and temporal variability in the sources
952 of suspended sediments in a Scottish mesoscale catchment. Sci. Total Environ. 755,
953 142916.

954 Huang, Y., Shuman, B., Wang, Y., Webb, T., 2004: Hydrogen isotope ratios of individual
955 lipids in lake sediments as novel tracers of climatic and environmental change: a
956 surface sediment test. J. Paleolimnol. 31, 363–375.

957 Huisman, J., Codd, G.A., Paerl, H.W., Ibelings, B.W., Verspagen, J.M.H., Visser, P.M., 2018:
958 Cyanobacterial blooms. Nat. Rev. Microbiol. 16, 471–483.

959 Irish, A.E., 1979: *Gymnodinium helveticum* Penard F. *Achroum* Skuja a case of phagotrophy.
960 *Brit. Phycol. J*. 14, 11–15.

961 Jankowiak, J., Hattenrath-Lehmann, T., Kramer, B.J., Ladds, M., Gobler, C.J., 2019:
962 Deciphering the effects of nitrogen, phosphorus, and temperature on cyanobacterial
963 bloom intensification, diversity, and toxicity in western Lake Erie. L&O 64, 1347–1370.

964 Jeng, W.-L., Huh, C.-A., Chen, C.-L., 1997: Alkanol and sterol degradation in a sediment
965 core from the continental slope off southwestern Taiwan. Chemosphere 35, 2515–
966 2523.

967 Jiang, M., Nakano, S.-I., 2022: The crucial influence of trophic status on the relative
968 requirement of nitrogen to phosphorus for phytoplankton growth. Water Res. 222,
969 118868.

970 Kassambara, A., 2023: ggcorrplot: Visualization of a Correlation Matrix using 'ggplot2'. R
971 package version 0.1.4.1. https://CRAN.R-project.org/package=ggcorrplot.

972 Kawamura, K., Ishiwatari, R., Ogura, K., 1987: Early diagenesis of organic matter in the
973 water column and sediments: Microbial degradation and resynthesis of lipids in Lake
974 Haruna. Org. Geochem. 11, 251–264.

975 Killops, S., Killops, V., 2004: Chemical Stratigraphic Concepts and Tools. in: Introduction to
976 Organic Geochemistry. Blackwell publishing company, Oxford, pp. 166-245.

977 Ladd, S.N., Dubois, N., Schubert, C.J., 2017: Interplay of community dynamics, temperature,
978 and productivity on the hydrogen isotope signatures of lipid biomarkers. Biogeosci.
979 14, 3979–3994.

980 Ladd, S.N., Nelson, D.B., Schubert, C.J., Dubois, N., 2018: Lipid compound classes display
981 diverging hydrogen isotope responses in lakes along a nutrient gradient. Geochim.
982 Cosmochim. Acta 237, 103–119.

983 Ladd, S.N., Nelson, D.B., Matthews, B., Dyer, S., Limberger, R., Klatt, A., Narwani, A.,
984 Dubois, N., Schubert, C.J., 2024: Taxon-specific hydrogen isotope signals in cultures
985 and mesocosms facilitate ecosystem and hydroclimate reconstruction. EarthArXiv,
986 7225.

987 Lammers, J.M., Schubert, C.J., Middelburg, J.J., Reichart, G.J., 2016: Carbon flows in
988 eutrophic Lake Rotsee: a ^{13}C-labelling experiment. Biogeochemistry 131, 147–162.

989 Lang, I., Hodac, L., Friedl, T., Feussner, I., 2011: Fatty acid profiles and their distribution
990 patterns in microalgae: a comprehensive analysis of more than 2000 strains from the
991 SAG culture collection. BMC Plant Biol 11, 124.

992 Leavitt, P.R., 1993: A review of factors that regulate carotenoid and chlorophyll deposition
993 and fossil pigment abundance. J. Paleolimnol. 9, 109–127.

Li, Y., Wu, S., Wang, L., Li, Y., Shi, F., Wang, X., 2010: Differentiation of bacteria using fatty acid profiles from gas chromatography–tandem mass spectrometry. J. Sci. Food Agric. 90, 1380–1383.

Liang, Z., Soranno, P.A., Wagner, T., 2020: The role of phosphorus and nitrogen on chlorophyll a: Evidence from hundreds of lakes. Water Res.185, 116236.

Lin, Q., Zhang, K., McGowan, S., Capo, E., Shen, J., 2021: Synergistic impacts of nutrient enrichment and climate change on long-term water quality and ecological dynamics in contrasting shallow-lake zones. L&O 66, 3271–3286.

Litchman, E., de Tezanos Pinto, P., Edwards, K.F., Klausmeier, C.A., Kremer, C., T., Thomas, M.K., 2015: Global biogeochemical impacts of phytoplankton: a trait-based perspective. J. Ecol. 103, 1384–1396.

Liu, M., Huang, Y., Hu, J., He, J., Xiao, X., 2023: Algal community structure prediction by machine learning. Environ. Sci. Ecotechnol. 14, 100233.

Lotter, A.F., 1998: The recent eutrophication of Baldeggersee Switzerland as assessed by fossil diatom assemblages. The Holocene 8, 395–405.

Lotter, A.F., 1989: Subfossil and modern diatom plankton and the paleolimnology of Rotsee Switzerland since 1850. Schweiz. Z. Hydrologie 51, 338–350.

M'Boule, D., Chivall, D., Sinke-Schoen, D., Sinninghe Damsté, J.S., Schouten, S., van der Meer, M.T.J., 2014: Salinity dependent hydrogen isotope fractionation in alkenones produced by coastal and open ocean haptophyte algae. Geochim. Cosmochim. Acta 130, 126–135.

Mancini, S.A., Ulrich, A.C., Lacrampe-Couloume, G., Sleep, B., Edwards, E.A., Sherwood Lollar, B., 2003: Carbon and Hydrogen Isotopic Fractionation during Anaerobic Biodegradation of Benzene. Appl. Environ. Microbiol. 69, 191–198.

Martin-Creuzburg, D., von Elert, E., 2004: Impact of 10 Dietary Sterols on Growth and Reproduction of *Daphnia galeata*. J. Chem. Ecol. 30, 483–500.

Martin-Creuzburg, D., von Elert, E., Hoffmann, K.H., 2008: Nutritional constraints at the cyanobacteria—*Daphnia magna* interface: The role of sterols. L&O 53, 456–468.

Martin-Creuzburg, D., Merkel, P., 2016: Sterols of freshwater microalgae: potential implications for zooplankton nutrition. J. Plankton Res. 38, 865–877.

Matsui, H., Shiozaki, K., Okumura, Y., Ishikawa, M., Waqalevu, V., Hayasaka, O., Honda, A., Kotani, T., 2020: Effects of phosphorus deficiency of a microalga *Nannochloropsis oculata* on its fatty acid profiles and intracellular structure and the effectiveness in rotifer nutrition. Algal Res. 49, 101905.

Mattern, J.P., Glauninger, K., Britten, G.L., Casey, J.R., Hyun, S., Wu, Z., Armbrust, E.V., Harchaoui, Z., Ribalet, F., 2022: A Bayesian approach to modeling phytoplankton population dynamics from size distribution time series. PLoS Comput. Biol. 18, e1009733.

McGowan, S., Barker, P., Haworth, E.Y., Leavitt, P.R., Maberly, S.C., Pates, J., 2012: Humans and climate as drivers of algal community change in Windermere since 1850. Freshw. Biol. 57, 260–277.

Michellod, D., Bien, T., Birgel, D., Violette, V., Kleiner, M., Fearn, S., Zeidler, C., Gruber-Vodicka, H.R., Dubilier, N., Liebke, M., 2023: De novo phytosterol synthesis in animals. Science 380, 520–526.

Miljević, N., Golobočanin, D., 2007: Potential Use of Environmental Isotopes in Pollutant Migration Studies. Arh. Hig. Rada. Toksikol. 58, 251–262.

Mouradian, M., Panetta, R.J., de Vernal, A., Gélinas, Y., 2007: Dinosterols or dinocysts to estimate dinoflagellate contributions to marine sedimentary organic matter? L&O 52, 2569–2581.

Muñoz-Marín, M.D.C., López-Lozano, A., Moreno-Cabezuelo, J.Á., Díez, J., García-Fernández, J.M., 2024: Mixotrophy in cyanobacteria. Curr. Opin. Microbiol. 78, 102432.

Narwani, A., Reyes, M., Pereira, A.L., Penson, H., Dennis, S.R., Derrer, S., Spaak, P., Matthews, B., 2019: Interactive effects of foundation species on ecosystem functioning and stability in response to disturbance. Proc R Soc B*:* Biol. Sci. 286, 20191857.

Naselli-Flores, L., Padisák, J., 2023: Ecosystem services provided by marine and freshwater phytoplankton. Hydrobiologia 850, 2691–2706.

Nelson, D.B., Ladd, S.N., Schubert, C.J., Kahmen, A., 2018: Rapid atmospheric transport and large-scale deposition of recently synthesized plant waxes. Geochim. Cosmochim. Acta 222, 599–617.

Nelson, D.B., Sachs, J.P., 2014: The influence of salinity on D/H fractionation in dinosterol and brassicasterol from globally distributed saline and hypersaline lakes. Geochim. Cosmochim. Acta 133, 325–339.

Newberry, S.L., Nelson, D.B., Kahmen, A., 2017: Cryogenic vacuum artifacts do not affect plant water-uptake studies using stable isotope analysis. Ecohydrology 10, e1892.

Not, F., Siano, R., Kooistra, W.H.C.F., Simon, N., Vaulot, D., Probert, I., 2012: Diversity and Ecology of Eukaryotic Marine Phytoplankton. Adv. Bot. Res. 64, 1–53.

Nwosu, E.C., Brauer, A., Monchamp, ME., Pinkerneil, S., Bartholomäus, A., Theuerkauf, M., Schmidt, J.-P., Stoof-Leichsenring, K.R., Wietelmann, T., Kaiser, J., Wagner, D., Liebner, S., 2023: Early human impact on lake cyanobacteria revealed by a Holocene record of sedimentary ancient DNA. Commun Biol 6, 72.

Oksanen, J., Simpson, G,., Blanchet, F., Kindt, R., Legendre, P., Minchin, P., O'Hara, R.B., Solymos, P., Stevens, M.H.H., Szoecs, E., Wagner, H., Barbour, M., Bedward, M., Bolker, B., Borcard, D., Carvalho, G., Chirico, M., De Caceres, M., Durand, S., Evangelista, H.B.A., FitzJohn, R., Friendly, M., Furneaux, B., Hannigan, G., Hill, M.O., Lahti, L., McGlinn, D., Ouellette, M.-H., Cunha, E.R., Smith, T., Stier, A., Ter Braak, C.J.F., Weedon, J., 2022: vegan: Community Ecology Package. R package version 2.6-4.

Osman, M.B., Tierney, J.E., Zhu, J., Tardif, R., Hakim, G.J., King, J., Poulsen, C.J., 2021: Globally resolved surface temperatures since the Last Glacial Maximum. Nature 599, 239–244.

Pal, S., Gregory-Eaves, I., Pick, F.R., 2015: Temporal trends in cyanobacteria revealed through DNA and pigment analyses of temperate lake sediment cores. J. Paleolimnol. 54, 87–101.

Pålsson, C., Granéli, W., 2004: Nutrient limitation of autotrophic and mixotrophic phytoplankton in a temperate and tropical humic lake gradient. J. Plankton Res. 26, 1005–1014.

Peltomaa, E., Asikainen, H., Blomster, J., Pakkanen, H., Rigaud, C., Salmi, P., S. Taipale, S., 2023: Phytoplankton group identification with chemotaxonomic biomarkers: In combination they do better. Phytochem. 209, 113624.

Peltomaa, E. T., Aalto, S. L., Vuorio, K. M., Taipale, S. J. 2017: The Importance of Phytoplankton Biomolecule Availability for Secondary Production. Front. ecol. evol. 5, 128.

Piepho, M., Martin-Creuzburg, D., Wacker, A., 2010: Simultaneous effects of light intensity and phosphorus supply on the sterol content of phytoplankton. PLoS ONE 5, e15828.

Piepho, M., Martin-Creuzburg, D., Wacker, A., 2012: Phytoplankton sterol contents vary with temperature, phosphorus and silicate supply: a study on three freshwater species. Eur. J. Phycol. 47, 138–145.

Piironen, V., Lindsay, D.G., Miettinen, T.A., Toivo, J., Lampi, A.-M., 2000: Plant sterols: biosynthesis, biological function and their importance to human nutrition.J. Sci. Food Agric. 80, 939–966.

Pilecky, M., Kämmer, S.K., Mathieu-Resuge, M., Wassenaar, L.I., Taipale, S.J., Martin-Creuzburg, D., Kainz, M.J., 2022: Hydrogen isotopes (δ^2H) of polyunsaturated fatty acids track bioconversion by zooplankton. Funct. Ecol. 36, 538–549.

Ptacnik, R., Solimini, A.G., Andersen, T., Tamminen, T., Brettum, P., Lepistö, L., Willén, E., Rekolainen, S., 2008: Diversity predicts stability and resource use efficiency in natural phytoplankton communities. PNAS 105, 5134–5138.

R Core Team, 2023: R: A Language and Environment for Statistical Computing. Vienna, Austria: R Foundation for Statistical Computing.

Rampen, S.W., Abbas, B.A., Schouten, S., Sinninghe Damste, J.S., 2010: A comprehensive study of sterols in marine diatoms Bacillariophyta: Implications for their use as tracers for diatom productivity. L&O 55, 91–105.

Reuss, N., Conley, D.J., Bianchi, T.S., 2005: Preservation conditions and the use of sediment pigments as a tool for recent ecological reconstruction in four Northern European estuaries. Mar. Chem. 95, 283–302.

Revelle, W., 2024: psych: Procedures for Psychological, Psychometric, and Personality Research. R package version 2.4.3. https://CRAN.R-project.org/package=psych.

Rontani, J.-F., Bonin, P.C., Volkman, J.K., 1999: Biodegradation of Free Phytol by Bacterial Communities Isolated from Marine Sediments under Aerobic and Denitrifying Conditions. Appl. Environ. Microbiol. 65, 5484–5492.

Rontani, J.-F., Volkman, J.K., 2003: Phytol degradation products as biogeochemical tracers in aquatic environments. Org. Geochem. 34, 1–35.

Rustan, A.C., Drevon, C.A., 2005: Fatty Acids: Structures and Properties, in: eLS. John Wiley and Sons, Chichester, UK.

Saad, J.F., Unrein, F., Tribelli, P.M., López, N., Izaguirre, I., 2016: Influence of lake trophic conditions on the dominant mixotrophic algal assemblages. J. Plankton Res. 38, 818–829.

Sachs, J.P., Kawka, O.E., 2015: The Influence of Growth Rate on $^2H/^1H$ Fractionation in Continuous Cultures of the Coccolithophorid *Emiliania huxleyi* and the Diatom *Thalassiosira pseudonana*. PLoS ONE 10, e0141643.

Sachs, J.P., Schwab, V.F., 2011: Hydrogen isotopes in dinosterol from the Chesapeake Bay estuary. Geochim. Cosmochim. Acta 75, 444–459.

Sachse, D., Billault, I., Bowen, G.J., Chikaraishi, Y., Dawson, T.E., Feakins, S.J., Magill, C.R., McInerney, F.A., van der Meer, M.T.J., Polissar, P., Robins, R.J., Sachs, J.P., Schmidt, H.-L., Sessions, A.L., White, J.W.C., West, J.B., Kahmen, A., 2012: Molecular Paleohydrology: Interpreting the Hydrogen-Isotopic Composition of Lipid Biomarkers from Photosynthesizing Organisms. Annu. Rev. Earth Planet. Sci. 40, 221–249.

Sauer, P.E., Eglinton, T.I., Hayes, J.M., Schimmelmann, A., Sessions, A.L., 2001: Compound-specific D/H ratios of lipid biomarkers from sediments as a proxy for environmental and climatic conditions. Geochim. Cosmochim. Acta 65, 213–222.

1137 Schimmelmann, A., Sessions, A.L., Mastalerz, M., 2006: Hydrogen isotopic D/H composition
1138 of organic matter during diagenesis and thermal maturation. Annu. Rev. Earth Planet.
1139 Sci. 34, 501–533.

1140 Schmidt, H.-L., Werner, R.A., Eisenreich, W., 2003: Systematics of ^{2}H patterns in natural
1141 compounds and its importance for the elucidation of biosynthetic pathways.
1142 Phytochem. Rev. 2, 61–85.

1143 Schouten, S., Ossebaar, J., Schreiber, K., Kienhuis, M.V.M., Langer, G., Benthien, A., Bijma,
1144 J., 2006: The effect of temperature, salinity and growth rate on the stable hydrogen
1145 isotopic composition of long chain alkenones produced by *Emiliania huxleyi* and
1146 *Gephyrocapsa oceanica*. Biogeosci. 3, 113–119.

1147 Schubert, C.J., Villanueva, J., Calvert, S.E., Cowie, G.L., von Rad, U., Schulz, H., Berner, U.,
1148 Erlenkeuser, H., 1998: Stable phytoplankton community structure in the Arabian Sea
1149 over the past 200,000 years. Nature 394, 563–566.

1150 Schwab, V.F., Garcin, Y., Sachse, D., Todou, G., Séné, O., Onana, J.-M., Achoundong, G.,
1151 Gleixner, G., 2015: Dinosterol δD values in stratified tropical lakes (Cameroon) are
1152 affected by eutrophication. Org. Geochem. 88, 35–49.

1153 Naeher, S., Smittenberg, R.H., Gilli, A., Kirilova, E.P., Lotter, A.F., Schubert, C.J., 2012:
1154 Impact of recent lake eutrophication on microbial community changes as revealed by
1155 high resolution lipid biomarkers. Org. Geochem. 49, 86–95.

1156 Serrazanetti, G.P., Conte, L.S., Pagnucco, C., Bergami, C., Milani, L., 1992: Sterol content in
1157 zooplankton of Adriatic Sea open waters. *Comp. Biochem. Physiol.* 102, 743–746.

1158 Shimoda, Y., Azim, M.E., Perhar, G., Ramin, M., Kenney, M.A., Sadraddini, S., Gudimov, A.,
1159 Arhonditsis, G.B., 2011: Our current understanding of lake ecosystem response to
1160 climate change: What have we really learned from the north temperate deep lakes? J.
1161 Great Lakes Res. 37, 173–193.

1162 Smol, J.P., 1985: The ratio of diatom frustules to chrysophycean statospores: A useful
1163 paleolimnological index. Hydrobiologia 123, 199–208.

1164 Summons, R.E., Welander, P.V., Gold, D.A., 2022: Lipid biomarkers: molecular tools for
1165 illuminating the history of microbial life. Nat. Rev. Microbiol. 20, 174–185.

1166 Taipale, S.J., Strandberg, U., Peltomaa, E., Galloway, A.W.E., Ojala, A., Brett, M.T., 2013:
1167 Fatty acid composition as biomarkers of freshwater microalgae: analysis of 37 strains
1168 of microalgae in 22 genera and in seven classes. Aquat. Microb. Ecol. 71, 165–178.

1169 Taipale, S.J., Hiltunen, M., Vuorio, K., Peltomaa, E., 2016: Suitability of Phytosterols
1170 Alongside Fatty Acids as Chemotaxonomic Biomarkers for Phytoplankton.
1171 Front. Plant Sci. 7, 212.

1172 Thorpe, A.C., Mackay, E.B., Goodall, T., Bendle, J.A., Thackeray, S.J., Maberly, S.C., Read,
1173 D.S., 2024: Evaluating the use of lake sedimentary DNA in palaeolimnology: A
1174 comparison with long-term microscopy-based monitoring of the phytoplankton
1175 community. Mol. Ecol. Resour. 24, e13903.

1176 Torres-Romero, I., Zhang, H., Wijker, R.S., Clark, A.J., McLeod, R.E., Jaggi, M., Stoll, H.M.,
1177 2024: Hydrogen isotope fractionation is controlled by CO_2 in coccolithophore lipids.
1178 PNAS 121, e2318570121.

1179 von Utermöhl, H., 1931: Neue Wege in der quantitativen Erfassung des Planktons. Mit
1180 besonderer Berücksichtigung des Ultraplanktons. Verh. Int. Verein. Theor. Angew.
1181 Limnol., 567–596.

1182 Vander Zanden, H.B., Soto, D.X., Bowen, G.J., Hobson, K.A., 2016: Expanding the Isotopic
1183 Toolbox: Applications of Hydrogen and Oxygen Stable Isotope Ratios to Food Web
1184 Studies. Front. ecol. evol. 4, 20.

1185 Vimeux, F., Masson, V., Jouzel, J., Stievenard, M., Petit, J.R., 1999: Glacial–interglacial
1186 changes in ocean surface conditions in the Southern Hemisphere. Nature 398, 410–
1187 413.

1188 Vogler, P., 1965: Beiträge zur Phosphatanalytik in der Limnologie. Die Bestimmung des
1189 gelösten Orthophosphates. Fortschr. Wasserchem. Grenzgeb. 2, 109–119.

1190 Volkman, J.K., 2003: Sterols in microorganisms. *Appl. Microbiol. Biotechnol.* 60, 495–506.

1191 Wacker, A., Martin-Creuzburg, D., 2012: Biochemical nutrient requirements of the rotifer
1192 *Brachionus calyciflorus*: co-limitation by sterols and amino acids. Funct. Ecol. 26,
1193 1135–1143.

1194 Weete, J.D., 1989: Structure and Function of Sterols in Fungi. Adv. Lipid Res. 23, 115–167.

1195 Wei, J.H., Yin, X., Welander, P.V., 2016: Sterol Synthesis in Diverse Bacteria.
1196 Front. microbiol. 7, 990.

1197 Wickham, H., 2009: ggplot2: Elegant Graphics for Data Analysis, second ed. Springer, New
1198 York.

1199 Wilke, C., 2020: cowplot: Streamlined Plot Theme and Plot Annotations for 'ggplot2'. R
1200 package version 1.1.1. https://CRAN.R-project.org/package=cowplot.

1201 Wille, E., Hoffmann, L., 1991: Population dynamics of the dinoflagellate *Gymnodinium*
1202 *helveticum* Penard in the reservoir of Esch-sur-Sûre G.-D. of Luxembourg. Belg. J.
1203 Bot. 124, 109–114.

1204 Witkowski, C.R., van der Meer, M.T.J., Blais, B., Sinninghe Damsté, J.S., Schouten, S.,
1205 2020: Algal biomarkers as a proxy for pCO_2: Constraints from late quaternary
1206 sapropels in the eastern Mediterranean. Org. Geochem. 150, 104123.

1207 Wittenborn, A.K., Schmale, O., Thiel, V., 2020: Zooplankton impact on lipid biomarkers in
1208 water column vs. surface sediments of the stratified Eastern Gotland Basin Central
1209 Baltic Sea. PLoS ONE 15, e0234110.

1210 Yuan, L.L., Pollard, A.I., 2018: Changes in the relationship between zooplankton and
1211 phytoplankton biomasses across a eutrophication gradient. L&O 63, 2493–2507.

1212 Yuan, Z., Liu, D., Masqué, P., Zhao, M., Song, X., Keesing, J.K., 2020: Phytoplankton
1213 Responses to Climate-Induced Warming and Interdecadal Oscillation in North-
1214 Western Australia. Paleoceanogr. Paleoclimatol. 35, e2019PA003712.

1215 Zagarese, H.E., Sagrario, M.D.L.Á.G., Wolf-Gladrow, D., Nõges, P., Nõges, T., Kangur, K.,
1216 Matsuzaki, S.-I.S., Kohzu, A., Vanni, M.J., Özkundakci, D., Echaniz, S.A., Vignatti, A.,
1217 Grosman, F., Sanzano, P., Van Dam, B., Knoll, L.B., 2021: Patterns of CO_2
1218 concentration and inorganic carbon limitation of phytoplankton biomass in
1219 agriculturally eutrophic lakes. Water Res. 190, 116715.

1220 Zeman-Kuhnert, S., Heim, C., Öztoprak, M., Thiel, V., 2023: Reconstructing eutrophication
1221 trends of a shallow lake environment using biomarker dynamics and sedimentary
1222 sterols. Org. Geochem. 177, S. 104555.

1223 Zhang, X., Gillespie, A.L., Sessions, A.L., 2009: Large D/H variations in bacterial lipids reflect
1224 central metabolic pathways. PNAS 106, 12580–12586.

1225 Zhang, Z., Sachs, J.P., 2007: Hydrogen isotope fractionation in freshwater algae: I.
1226 Variations among lipids and species. Org. Geochem. 38, 582–608.

1227 Zhang, Z., Sachs, J.P., Marchetti, A., 2009: Hydrogen isotope fractionation in freshwater and
1228 marine algae: II. Temperature and nitrogen limited growth rate effects. Org.
1229 Geochem. 40, 428–439.

1230

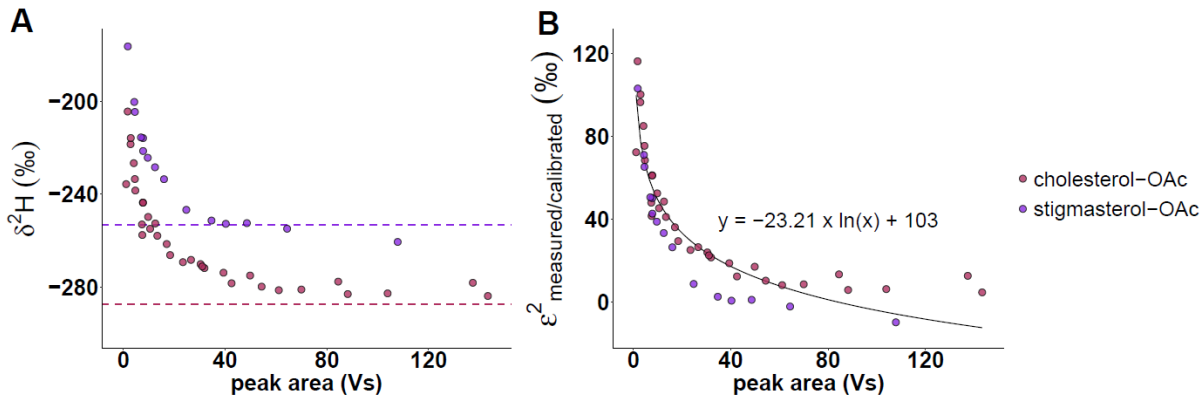

Figure S1: Relationship between measured and calibrated δ^2H values and peak area dimension of cholesterol acetate (cholesterol-OAc) and stigmasterol acetate (stigmasterol-OAc) standards. (A) Relationship between measured δ^2H values and peak area. δ^2H values derived from calibration against reference H_2 gas without further conversion. Dashed lines indicate calibrated δ^2H values based on TC/EA IRMS (cholesterol-OAc) or mean δ^2H values sufficient peak area (stigmasterol-OAc). (B) Relationship between $\varepsilon^2_{measured/calibrated}$ values and peak area with corresponding formula.

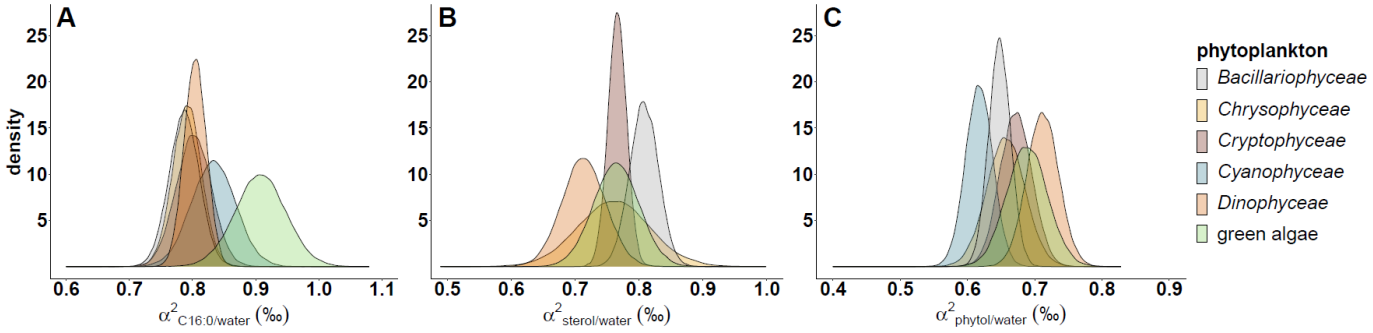

Figure S2: Theoretical distributions of $\alpha^2_{C16:0/water}$ values (A), $\alpha^2_{sterol/water}$ values (B), and $\alpha^2_{phytol/water}$ values (C) of different phytoplankton groups based on batch cultures from Ladd *et al.* (2024). Densities were determined by Monte Carlo simulation (n = 50,000) of normal distributions with mean and standard deviation from culturing $\alpha^2_{lipid/water}$ values (Ladd *et al.,* 2024). *Chlorophyceae* and *Zygnemopyceae* were summarized to the higher classification 'green algae'. For *Chrysophyceae*, $\alpha^2_{lipid/water}$ values distributions were simulated based on *Bacillario-and Dinophyceae* due to missing culturing data. No $\alpha^2_{sterol/water}$ values were defined for *Cyanophyceae* due to the lack of sterol production.

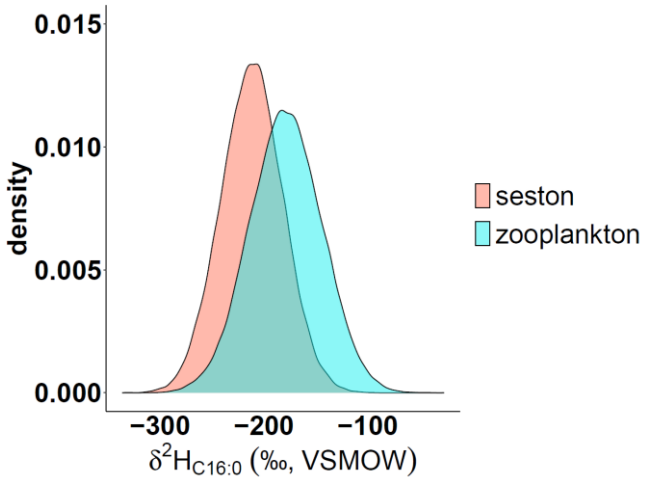

Figure S3: Theoretical distribution of $\delta^2H_{C16:0}$ values of seston and zooplankton based on field data from Pilecky *et al.*, 2022. Densities were determined by Monte Carlo simulation (n = 50,000) of normal distributions with mean and standard deviation from field $\delta^2H_{C16:0}$ values (Pilecky *et al*., 2022).

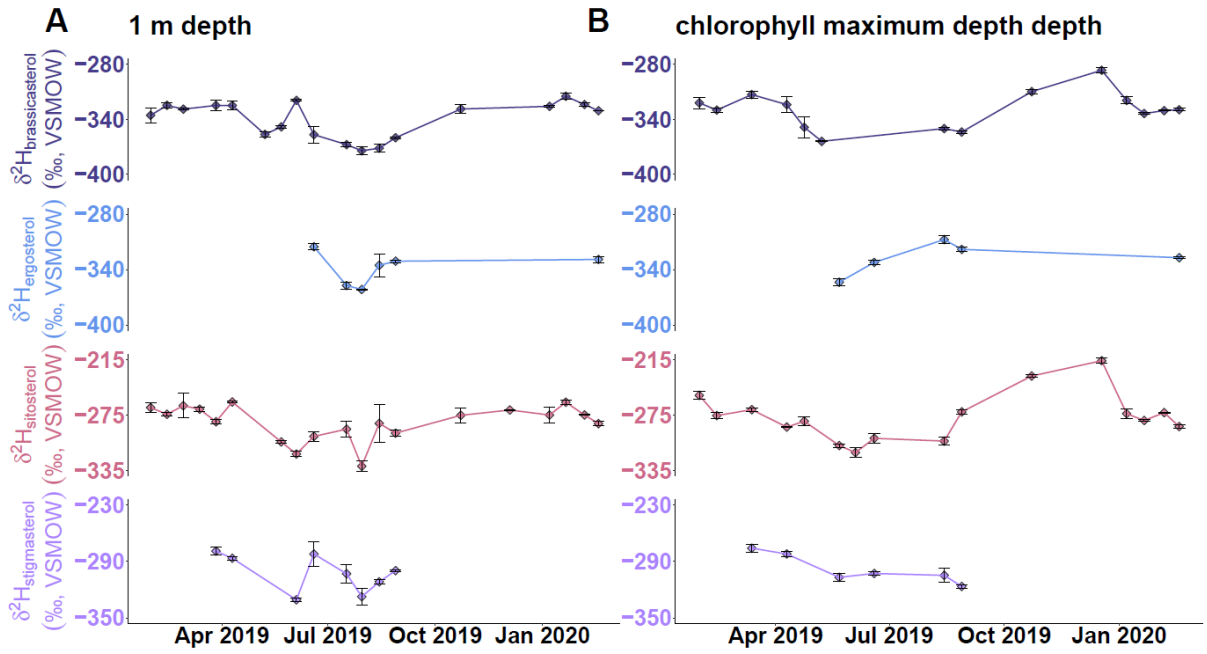

Figure S4: Time series of $\delta^2H_{brassicasterol}$, $\delta^2H_{ergosterol}$, $\delta^2H_{sitosterol}$ and $\delta^2H_{stigmasterol}$ values in Rotsee at 1 m depth (A) and chlorophyll maximum depth (B).

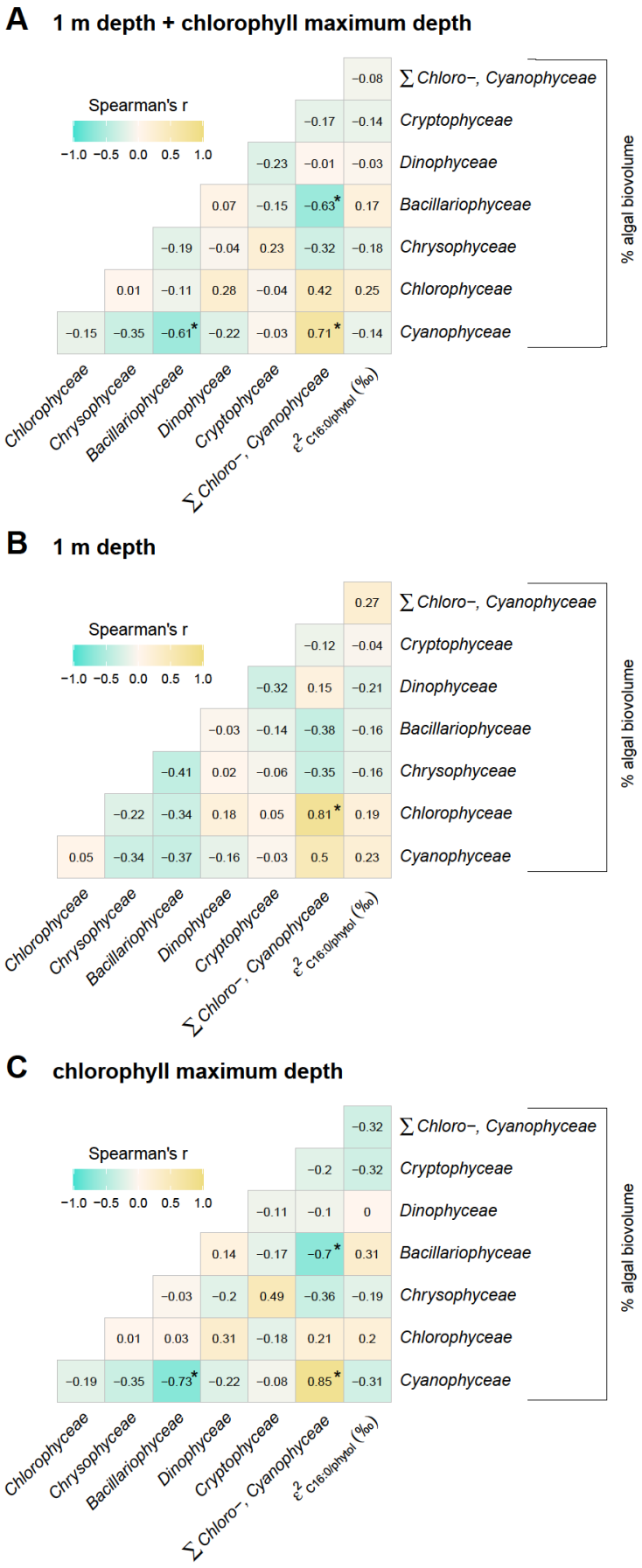

Figure S5: Correlation matrix indicating Spearman's correlations between $\varepsilon^2_{C16:0/phytol}$ values and the relative biovolume of individual phytoplankton groups in Rotsee combining both sampling depths (A), or at 1 m depth (B) and the chlorophyll maximum depth (C) analyzed separately. r: correlation coefficient. *: $P < 0.05$.

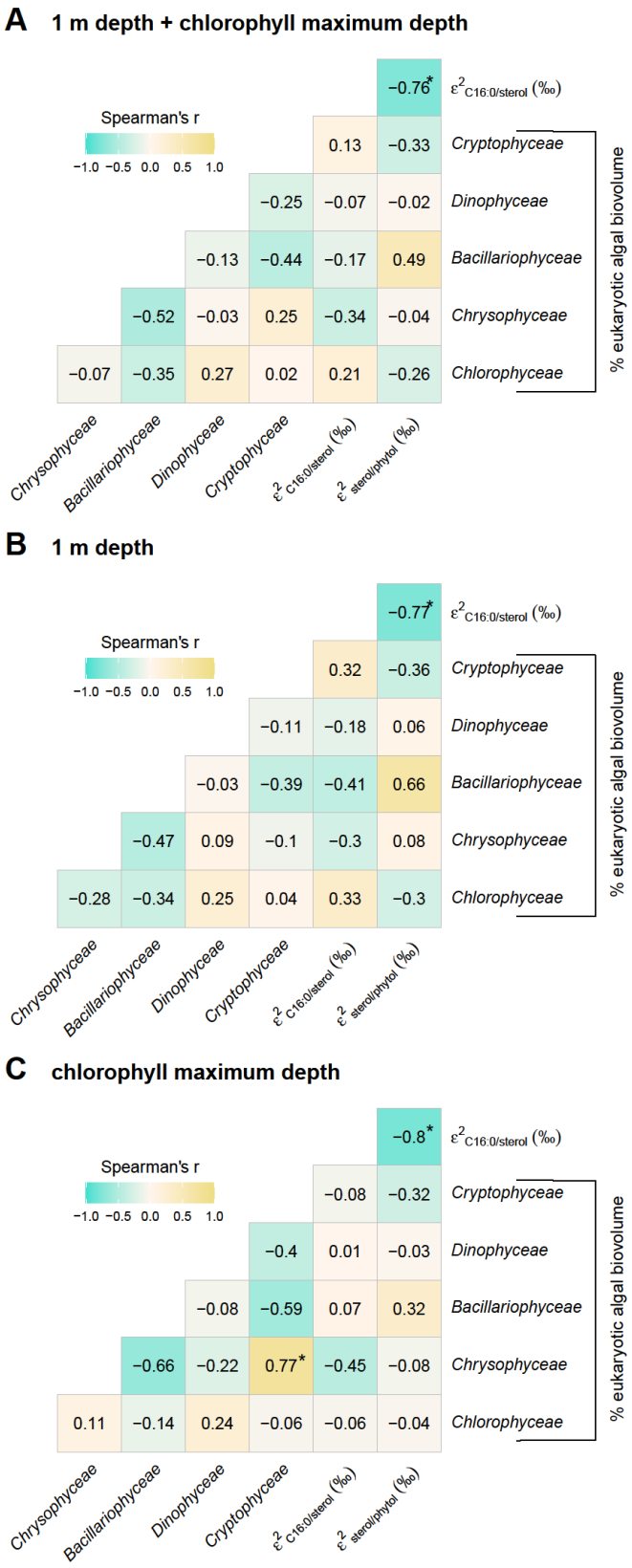

Figure S6: Correlation matrix indicating Spearman's correlations between $\varepsilon^2_{C16:0/sterol}$ and $\varepsilon^2_{sterol/phytol}$ values and the relative biovolume of individual eukaryotic algal groups in Rotsee combining both sampling depths (A), or at 1 m depth (B) and the chlorophyll maximum depth (C) analyzed separately. Relative contributions from single algal groups to eukaryotic algal biovolume were calculated excluding cyanobacteria. r: correlation coefficient. *: $P < 0.05$.

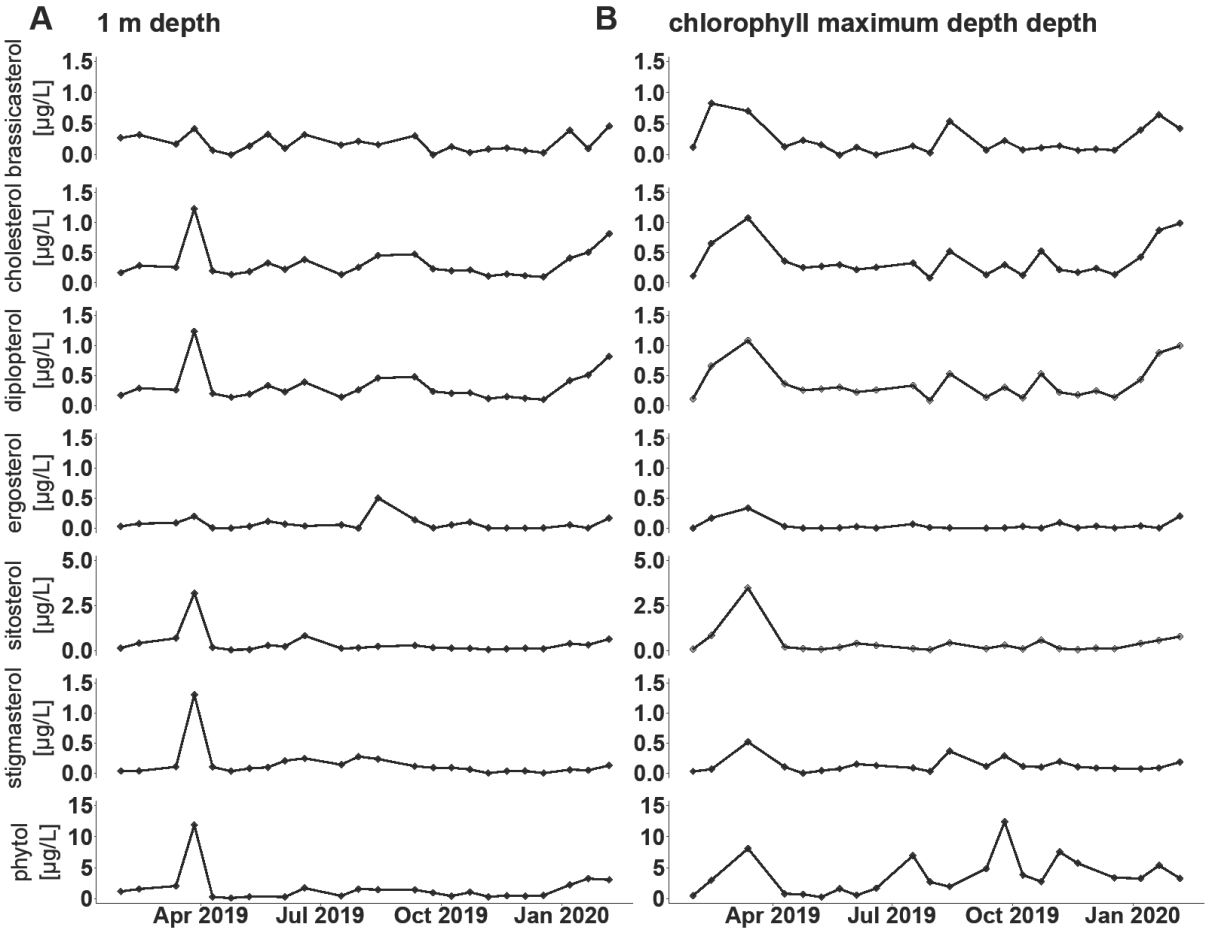

Figure S7: Time series of alcohol concentrations in Rotsee at 1 m depth (A) chlorophyll maximum depth (B). Note the different scaling of y-axes for individual alcohols.

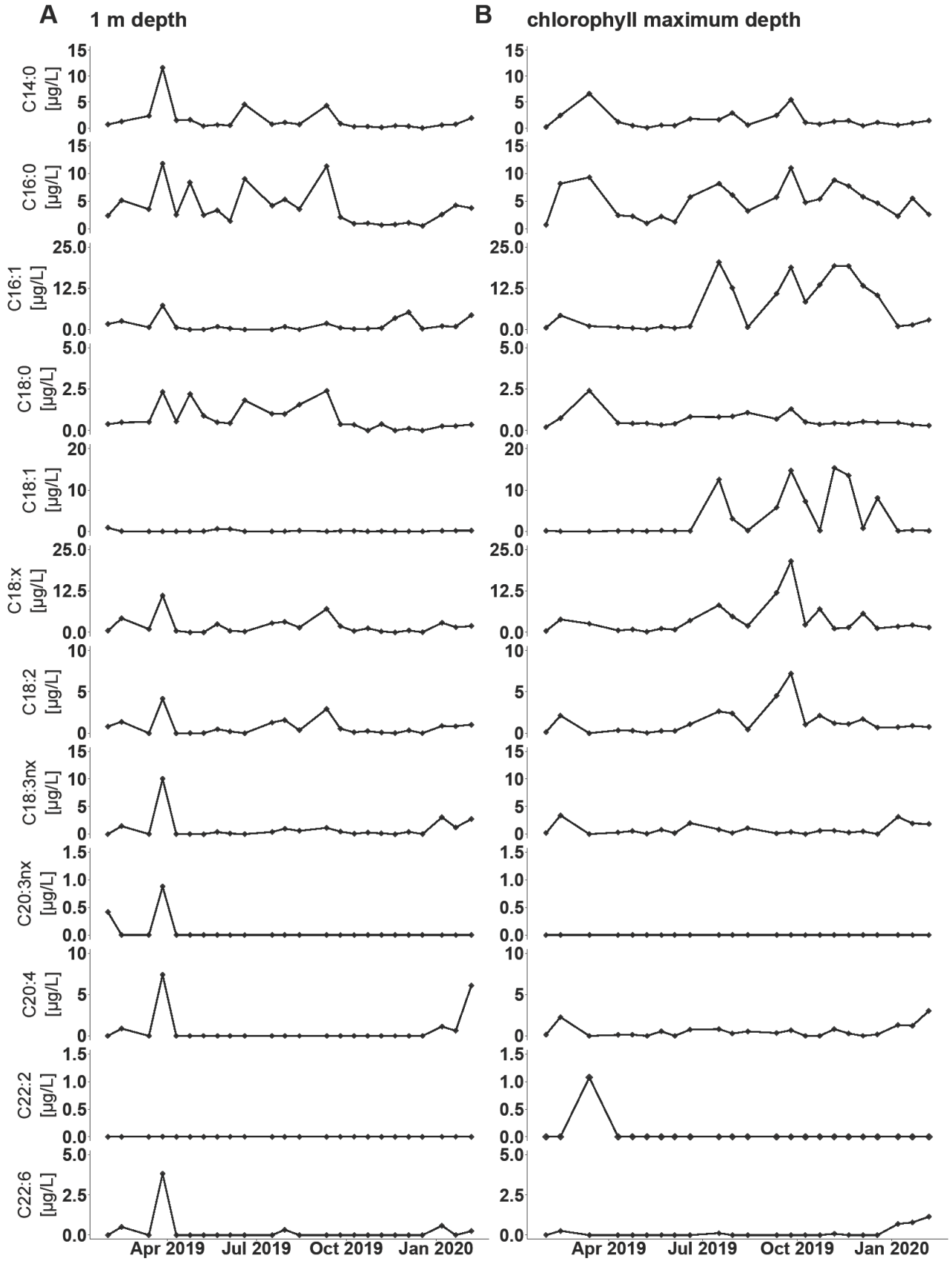

Figure S8: Time series of fatty acid concentrations in Rotsee at 1 m depth (A) and chlorophyll maximum depth (B). Note the different scaling of y-axes for individual fatty acids.

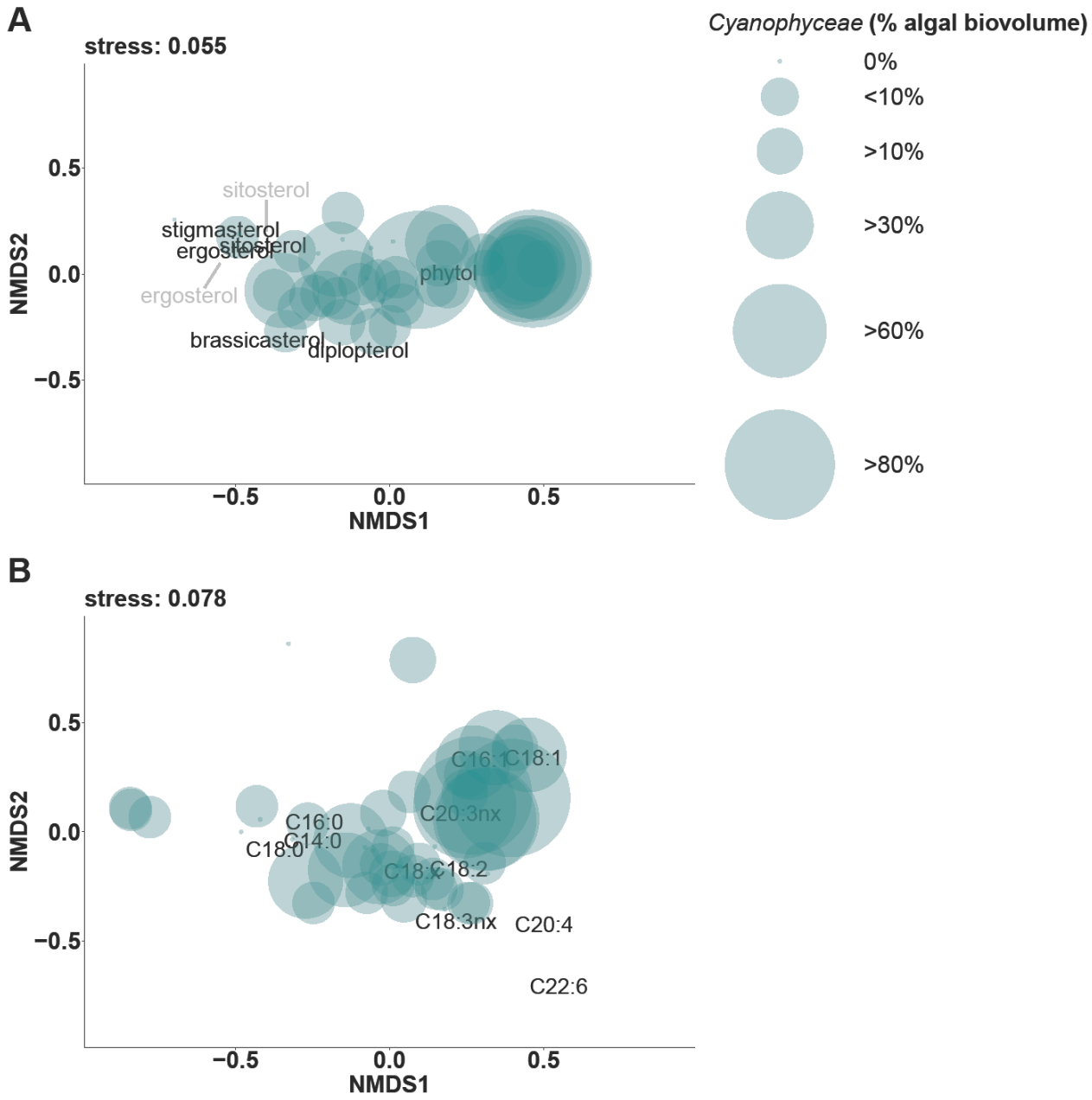

Figure S9: Non-metric-multidimensional scaling (NMDS) of relative alcohol and fatty acid concentrations in the water column of Rotsee. The ordination was set to k=3 dimensions and only the first and second dimensions are shown (NMDS1 vs. NMDS2)). Size scaling of each sample point is based on the relative contribution of cyanobacteria to total phytoplankton biovolume. (A) NMDS of untransformed relative alcohol concentrations. NMDS is based on relative contributions of brassicasterol, diplopterol, ergosterol, phytol, sitosterol and stigmasterol to total alcohol concentrations at single sampling dates, with a final stress of 0.055. (B) NMDS of square root transformed relative fatty acid concentrations. NMDs is based on relative contributions of C14:0, C16:0, C16:1, C18:0, C18:2, C18:3, C18:3nx, C18:x, C20:3nx, C20:4, and C22:6 to total fatty acid concentrations at single sampling dates, with a final stress of 0.078.

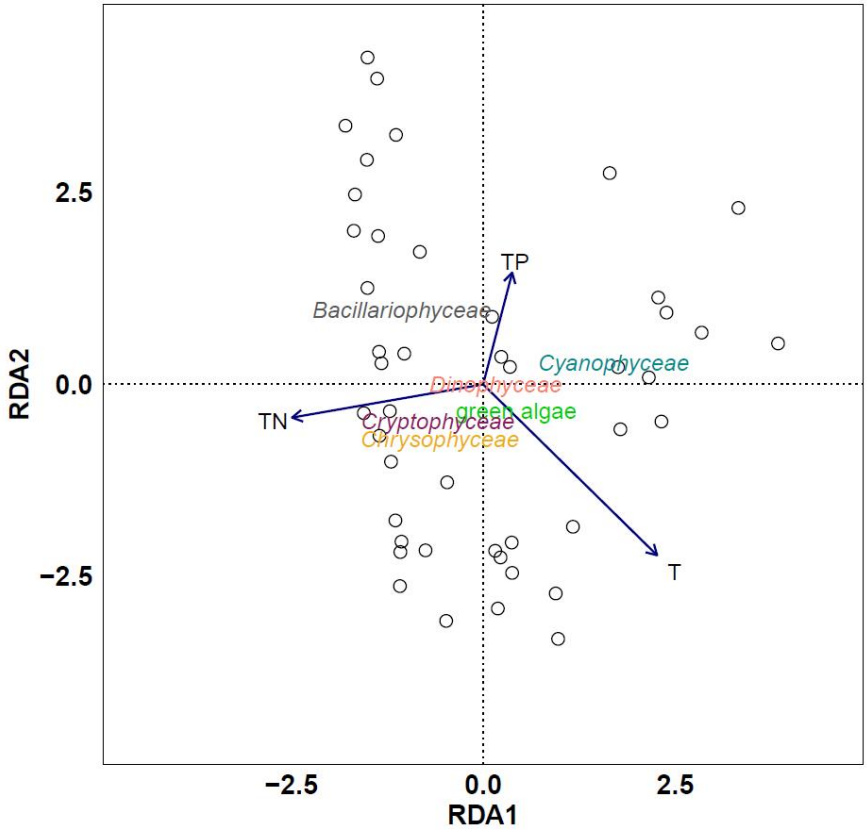

Figure S10: Redundancy analysis (RDA) of relative phytoplankton biovolume and environmental variables (total nitrogen (TN), total phosphorus (TP) and temperature (T)) in Rotsee. Relative biovolume of phytoplankton groups was square root transformed and total phosphorous concentrations were log transformed. TN, TP and T together explained 19.85 % of variance in phytoplankton biovolume ($p = 0.001$). Environmental variables were significantly correlated with each other (TN – TP: $r = 0.5$ $p < 0.001$; TN – T: $r = -0.6$ $p < 0.0001$; TP – T: $r = -0.5$ $p < 0.01$).